EVALUATION OF EMPIRICAL WAVELET TRANSFORMS FOR GLAUCOMA DETECTION USING FUNDUS IMAGES

Thesis submitted in partial fulfillment of the requirements for the Degree of

MASTER OF TECHNOLOGY

By

SHILPA KAUSHAL
Enrollment No: 162004

UNDER THE GUIDANCE OF
DR. SHRUTI JAIN
AND
DR. SUNIL DATT SHARMA

Department of Electronics and Communication Engineering

JAYPEE UNIVERSITY OF INFORMATION TECHNOLOGY, WAKNAGHAT
May-2018

TABLE OF CONTENTS

DECLARATION BY THE SCHOLAR

I hereby declare that the work reported in the M-Tech thesis entitled **"EVALUATION OF EMPIRICAL WAVELET TRANSFORMS FOR GLAUCOMA DETECTION USING FUNDUS IMAGES"** submitted at **Jaypee University of Information Technology, Waknaghat India,** is an authentic record of my work carried out under the supervision of **Dr. Shruti Jain and Dr. Sunil Datt Sharma.** I have not submitted this work elsewhere for any other degree or diploma.

Shilpa Kaushal

Department of Electronics and Communication Engineering
Jaypee University of Information Technology, Waknaghat, India

Date:

CERTIFICATE

This is to certify that the work reported in the M.Tech project report entitled **"EVALUATION OF EMPIRICAL WAVELET TRANSFORMS FOR GLAUCOMA DETECTION USING FUNDUS IMAGES"** which is being submitted by **Shilpa Kaushal** in fulfillment for the award of Masters of Technology in Electronics and Communication Engineering by the Jaypee University of Information Technology, is the record of candidate's own work carried out by him under my supervision. This work is original and has not been submitted partially or fully anywhere else for any other degree or diploma.

Dr. Shruti Jain

Associate Professor

Department of Electronics & Communication Engineering

Jaypee University of Information Technology, Waknaghat

Dr. Sunil Datt Sharma

Assistant Professor (Sr. Grade)

Department of Electronics & Communication Engineering

Jaypee University of Information Technology, Waknaghat

LIST OF FIGURES

LIST OF TABLES

ACKNOWLEDGEMENT

LIST OF ACRONYMS & ABBREVIATIONS

EWT   Empirical Wavelet Transform

DWT   Discrete Wavelet Transform

POAG   Primary Open-Angle Glaucoma

CDR   Cup-to-Disk Ratio

SVM   Support Vector Machine

OCT   Optical Coherence Tomography

ANN   Artificial Neural Network

DFT   Discrete Fourier Transform

FPS   Fourier Power Spectrum

GA   Genetic Algorithm

GLCM   Gray Level Co-occurrence Matrix

GLDS   Gray Level Difference Statistics

GWT   Gabor Wavelet Transform

K-NN   K- Nearest Neighbor

MTANN   Massive Training Artificial Neural Network

NGTDM   Neighborhood Gray Tone Difference Matrix

NN   Neural Network

PDF   Probability Distribution Function

RMSE   Root Mean Square Error

ABSTRACT

Glaucoma, a multi factor optical neuropathy, harms the optic nerve fibers impairing the vision and finally leads to blindness. Often titled as 'The sneak thief of Sight', Glaucoma has no significantly identifiable symptoms until considerable vision loss has occurred. Affecting one in every two hundred of the population younger than fifty and one in ten in the population aged above eighty, Glaucoma ranks second in the count of diseases causing blindness all around the globe. In the present scenario of technological and medical advancements, Computer vision and image processing form an imperative field of modern Ophthalmology. Medical imaging has delved into the deepest corners of the field and provided efficient healthcare services at appropriate prices in almost all disease areas. The less invasive techniques provided by medical imaging provides scientists and physicians with important information that could be life-saving. New imaging techniques used for retinal analysis are computationally complex, expensive and have poor performance parameters. Therefore, there is a need to be develop a less expensive, low computational complex, non-invasive and efficient method for the detection of Glaucoma. The objective of this work is to emphasize on the signal processing methods for the early detection of Glaucoma. This study aims to automatically differentiate fundus images of normal eye from Glaucoma eye on the basis of structural feature and distribution of textures. The method used for the detection of Glaucoma is based on empirical wavelet transform (EWT). Decomposition of image is done using EWT and correntropy values are calculated from these decomposed components. These extracted features are ranked based on student t-test value. Then, these features are used for the classification of normal and glaucoma images using SVM classifier. We have compared results of different types of EWT Transforms i.e. EWT 2D Little-wood Paley, EWT 2D Curvelet, EWT 2D Ridgelet and EWT 2D Tensor.

CHAPTER-1

INTRODUCTION

Glaucoma is an optic nerve disease which results in the blindness. The main cause of Glaucoma is increase in intraocular pressure of the eye. To study the disease in detail knowledge of the human eye and various diseases of the eye is required.

1.1 HUMAN EYE

The eye is a vital and a standout amongst the most complex sense organ that we people are enriched with. It causes us in envisioning objects. [1]. Henceforth it is essential to comprehend the structure and working of a human eye.

1.1.1 STRUCTURE OF HUMAN EYE

A human eye is approximately a circular ball. It comprises of the accompanying parts [1]:

1. **Tear Layer**: It is the first layer of the eye which is clear, moist and salty in nature. The main function of this layer is to maintain the smoothness and moisture in the eye.

2. **Cornea**: It is the part of the eye where light strikes first. It is the sensible, open front portion of the eye which gives protection to the iris and contributes in the eye's optical power as it focalize the light beams entering in the eye. When optical power is low then that condition is termed as farsightedness and when it is excessively soak results in partial blindness.

3. **Anterior Chamber**: It is filled with Aqueous Humor which is a sensible, watery liquid that fills the space present between the cornea back surface and vitreous front surface. It supplies oxygen to the eye and provides shape to the eye. It helps eye to work properly by supplying proper nutrition to the cornea, iris and retina.

4. **Iris**: It is the pigmented tissue like a diaphragm of the camera which lies behind the cornea and provides shading in the eye by controlling the amount of light which enters the eye. The main purpose of the eye is to adjust the size of the pupil.

5. **Pupil**: It is part of eye present in front of the iris. It keeps the check on the amount of light that enters the eye. When the intensity of light is very high, it contrasts and expands

when intensity is low. It is black in color as the light which enters through pupil doesn't reflect back.

6. **Lens**: It is located in the back of pupil and responsible for the focus of eye on the small details in the surroundings. It is transparent, biconvex intraocular tissue. It change its thickness to accommodate the details of the things present around. But with the age, it loses its elasticity so it can focus well resulting in many eye disorders like cataract and presbyopia.

7. **Ciliary Body**: It is a ring of tissue present between the end of the choroids and the beginning of the iris consists of the ciliary muscle which are responsible for the lens accommodation and maintain the intraocular pressure of the eye.

8. **Vitreous Humour** : It is the transparent, colorless jellylike quantity that fills two-third of the eyeball between the lens and the retina. As it is colorless in nature, light passes directly through it. Its presence is very essential otherwise if not present, then eye will collapse.

9. **Retina**: It is the light sensitive nerve tissue present in the eye. It converts the images formed by the lens into electrical impulses and then pass them optic nerve which is connected to the brain for the interpretation of the image as a vision. It is made of numerous cells which are light receptors. There are only two types of light receptors present in the retina namely cones and rods. At the junction of the retina and optic nerve, there are no light receptors so that point is termed as blind spot.

10. **Sclera**: It is the cloudy, strong and self-protective external layer of the eye or the white portion of the eye covering the optic nerve. It provides the security and border the inner parts of the eye.

11. **Optic Nerve:** The Optic Nerve is the nerve located at the end of the eye. Its main function is to transfer the data from the retina through the cones and rods to the brain. Without the presence of optic nerve, vision is not possible.

Human Eye
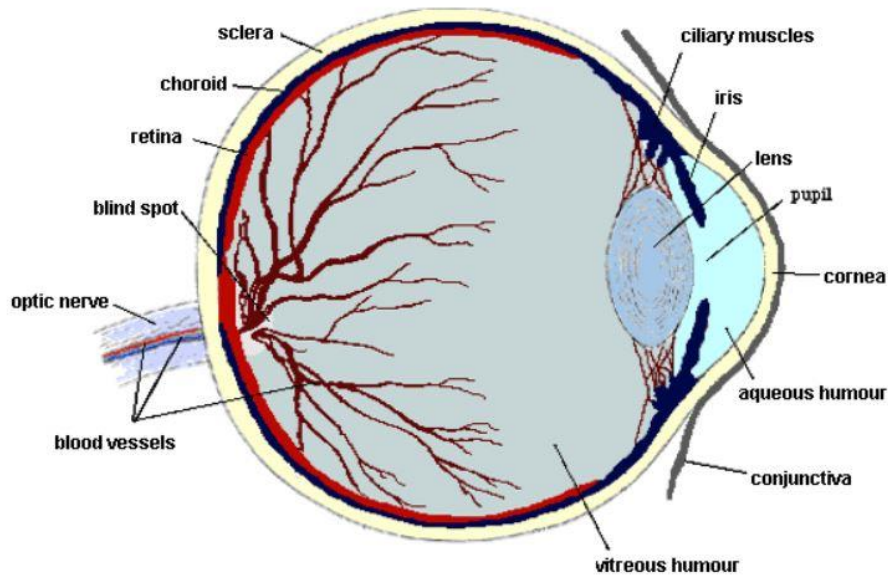
Figure 1. 1 Structure of Eye [2]

1.2 DISEASES:

A disease is a condition in which illness in the any part in the living organism is not due to the external injury. Pathology is the study of diseases and its cause. [1].

Different Diseases of Eye: The vision impairment in the eye is due to the harm or consequence of damage in any part of the eye. The damage may influence the way the eye gets or frames the visual data. Second, the eyeball might be proportioned mistakenly (have unexpected measurements in comparison to normal), making the eyeball harder to center on objects or might not the growth is done accurately. As a results, the piece of the mind that produces visual data may not work appropriately [3]. Different diseases of eye are discussed below:

1. **Age Related Macular Degeneration**: It is a physical distressing effect that affects the focal point of the retina called macula. It is the part of the eye which is responsible for our intense vision that is required for sharp and fine vision.

3
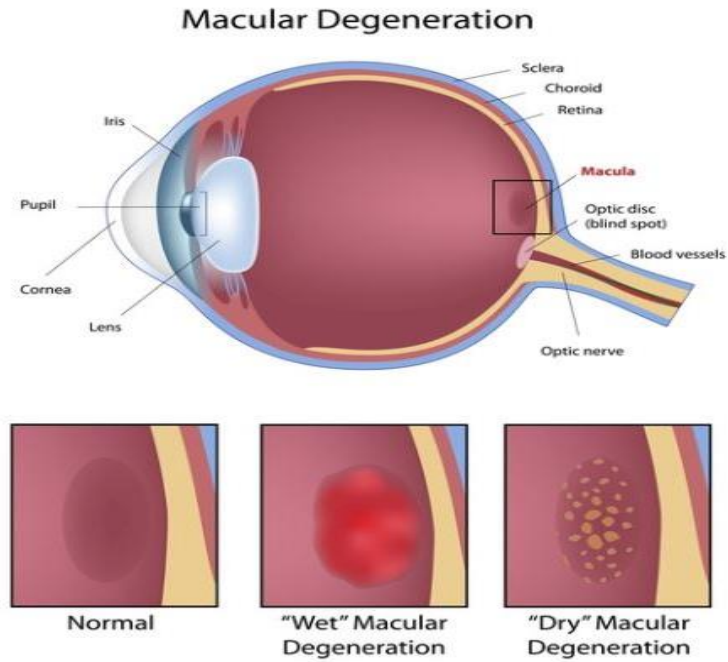
Figure 1.2: Age Related Macular Degeneration [4]

2. **Uveitis**: The uvea is a vascular and strong layer that secures the eye that provides nourishment and helps in gas trade in the eye. It is divided into 3 parts namely iris, choroid and ciliary body. Uveitis is the aggravation in the any section of the uvea.
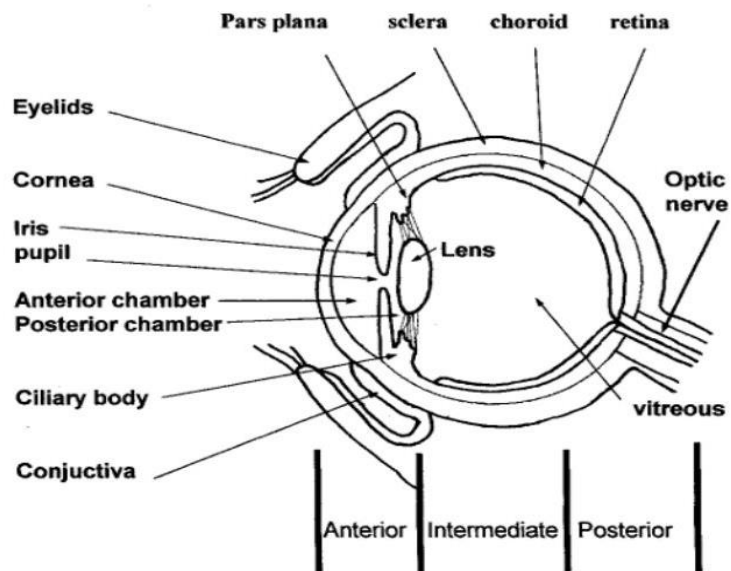
Figure 1.3: Uveitis affected eye image of the person [4]

3. **Cataract**: With the increasing age, development of the cataract is prominent due to the change in natural crystalline lens. The focus of the eye is disturbed due to the loss in

flexibility of lens. Development of cataract in children in their early age is a very rare case.
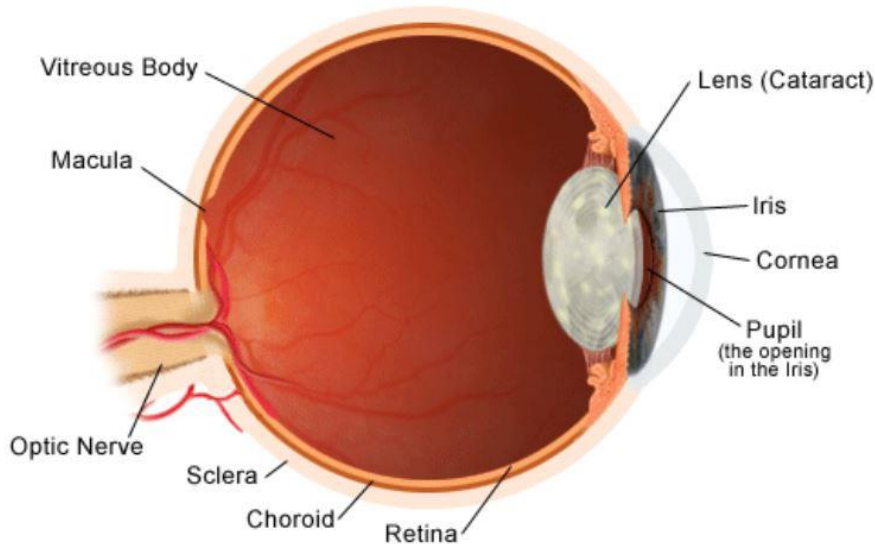
Figure 1.4: Cataract [4]

4. **Color Blindness**: Difficulty in differtianting certain colors but ablility to see is the condition which is known as "color blindness". Every individual who is color blind do not have problem in the differentiation of similar colors. Some of them cannot differentiate between red and green in low light whereas some people cannot distinct blues from yellows. Few people also suffer from the monochromatic condition that allows them to see only black and white color. The rate of color blindness is higher in men than women.
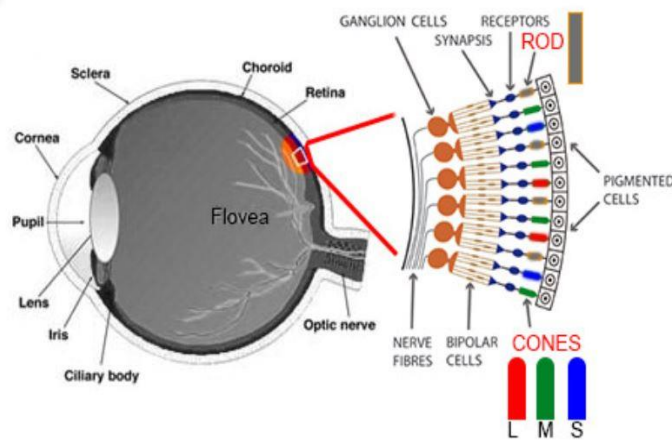
Figure 1.5: Color Blindness [5]

5. **Diabetic macular Oedema:** The macula is the part of the eye which is filled with photoreceptors i.e. cones which are responsible for the light sensing. When it starts to fill with fluid in the macula then their capability to sense light is hindered which result in the blurness. Approximately 30% diabetic people are suffering from this disease. Out of 20 to 30% of people experience moderate vision loss.
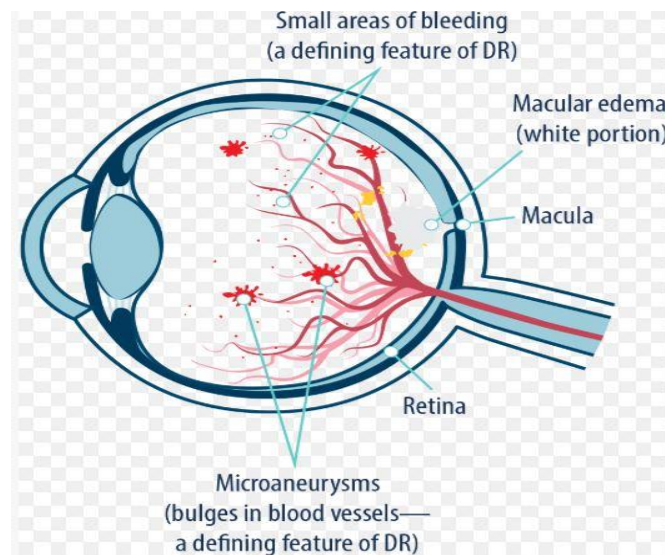
Figure 1.6: Diabetic macular Oedema [5]

6. **Eye Floaters and eye Flashes**: Eye floaters are tiny spots that floats in front of the eye are actually the shadows of cells and fibers present inside the aqueous humor of the eye. It is an isolated occurrences that are a perfectly normal part of vision.
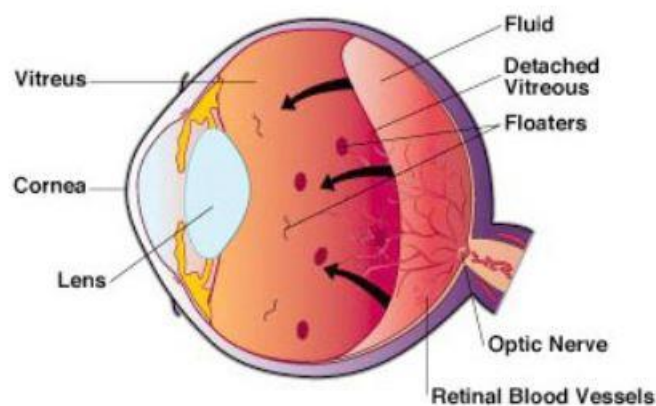
Figure 1.7: Eye Floaters [5]

7. **Glaucoma:** It is the condition in the eye that damages the optic nerve due to the increase in intraocular pressure of the eye. The ultimate result of this disease is blindness as it is unrecognizable at the early stage.

8. **Keratoconus:** Irregularity in the shape of the cornea prevents the focus of light beam in retina is termed as keratoconus. In this condition the shape of cornea changes to cone from round shape leading to sensitivity to bright light and blurness in the eye.
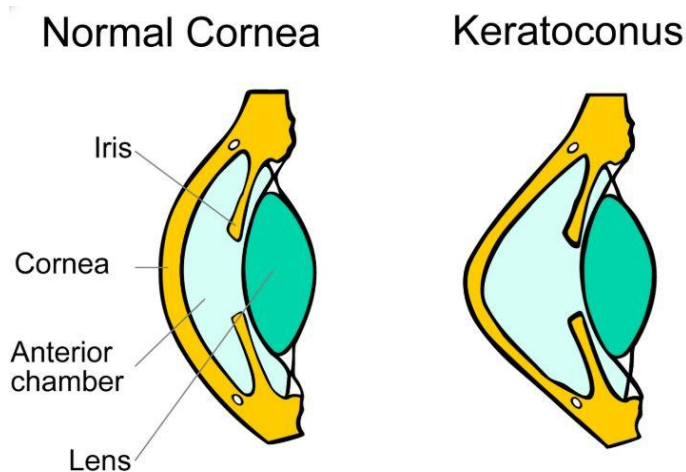
Figure 1.8: Keratoconus [6]

9. **Ocular Hypertension:** When the IOP range is above 21mm Hg that is considered as normal range of IOP becomes the main cause of ocular hypertension in the eye. It is worst condition than glaucoma as there are no detectable symptoms and damage to optic nerve is not irreversible. Patients having this disease are more prone to Glaucoma.
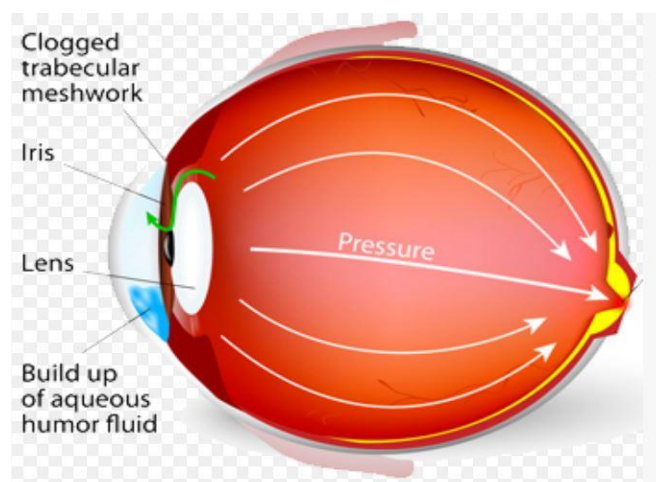
Figure 1.9: Ocular Hypertension [7]

10. Retinal Detachment: It is the condition when the retina is separated from the nerve tissues and blood supply. It has clouding effect in the eye. It can be treated if detected early.
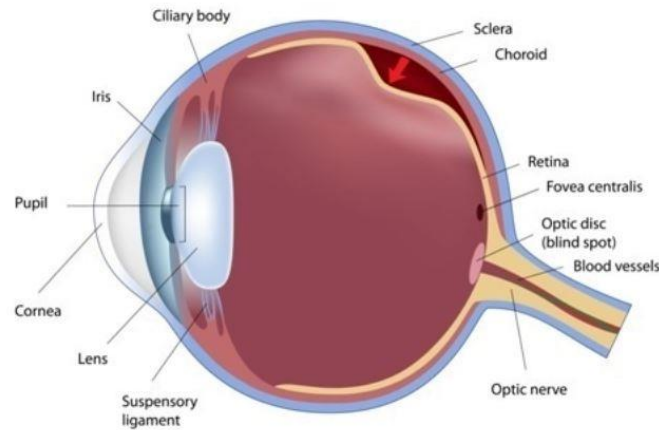
Figure 1.10: Retinal Detachment [8]

After the study of various disease of the eye, we have chosen Glaucoma in our thesis work. Glaucoma is the primary cause of blindness around the globe. The person suffering from glaucoma is also prone to many diseases like Cataract, Color blindness, Diabetic retinopathy etc.

1.2   GLAUCOMA

People about 6 to 67 million have glaucoma globally [9]. Every year more than 2 million people are affected by Glaucoma in USA. Glaucoma mostly occurs at the age of 40. Glaucoma has been referred to as the "silent thief of sight" because the vision of loss that occurs slowly and increasingly with no symptoms and warning signs. Globally, glaucoma is the second-leading cause of blindness behind cataracts [10]. In 2010, in all around the world there are 44.7 million people suffered with open angle glaucoma. By 2020, the frequency is estimated that increase to 58.6 million universal [11]. Women are more prone to Closed-angle glaucoma. Loss of bilateral vision can harmfully affect the mobility and interfere through driving. People with primary open angle glaucoma must increase the rates of mortality, or risk of cardiovascular death also increased. Early detection of Glaucoma can decrease the probability of total blindness in the

remote areas due to the no prior knowledge of the early symptoms of the Glaucoma and absence of methods used for the detection.

Glaucoma, an optic nerve disease occurs due to variation i.e. increase or decrease in fluid pressure within the eye. The pressure of the normal eye is 21 mm of Hg and when the pressure value is higher than 21 mmHg or 2.8 kPa, the optic nerve gets damaged leading to vision impairments .[7]

Diagnosis and treatment is based on elevation of Intraocular Pressure (IOP). The nerve cells are compressed due to the pressure that is buildup in the eye that eventually leads to permanent vision loss. Cornea is filled by aqueous humor which nourishes the lens and cornea with nutrients, oxygen and provides optimal pressure known as IOP that preserve the shape of the eye. IOP is measured for detecting glaucoma and diagnosis is done by dilated eye examination showing an abnormal amount of cupping shown in Figure 1.11b [9]. When the sight is lost which is the initial sign of Glaucoma where it is unrecognized. Vision loss, seeing halos around lights, eye that looks hazy, redness in the eye, vision loss are the post symptoms of Glaucoma. [6].
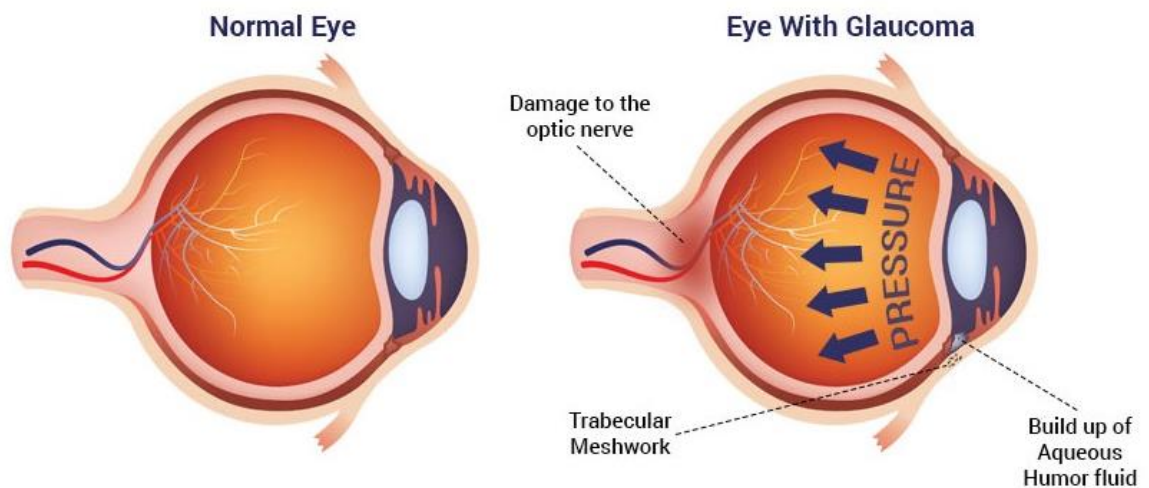
Figure 1.11: Normal eye vs Glaucoma eye [5]

1.3.1 History of Disease

In ancient medicine literature [9], Hippocrates has explained "glaykoseis" as the condition of blindness that happens in the elderly. The first English ophthalmologist who marked the connection between raised pressure of the eyeball and glaucoma was Richard Banister (1622)

in his book "Banister's Breviary of the Eyes,"[12].The term 'Glaucoma' was first coined by Hippocrates approximately 400 BC. In the Hippocratic "Aphorisms" the term was used to explain the blindness that would be explained in years that was connected with a glassy look of the pupil. The definition of glaucoma has changed with the time. The first detection of this disorder is related with the increase in IOP and that is now known as Glaucoma available in the Arabian writings, "Book of Hippocratic treatment", of At-Tabari (10th century).

In 1818 the French physician Antoine-Pierre Demours for the first time provided a brilliant explanation of glaucoma with increased ocular tension. As indicated by current understanding of Glaucoma, it states to a heterogeneous class of optic neuropathies having a complex genetic basis. It is a multifactorial optic disc neuropathy in which there is a trademark gained loss of RGCs and decay of the optic nerve. These neuropathies steadily diminish vision frequently all of a sudden without any symptoms. At least half of the affected people are uninformed about the disease making glaucoma a primary cause of irreversible visual deficiency.

1.3.2   Risk Factors of Glaucoma

There are the factors which are responsible for the occurrence of Glaucoma in the person are age above 60, family history of glaucoma, eye injuries, eye surgeries, decrease in the thickness of the cornea, low blood pressure, diabetics, migraines, increase in intra-ocular pressure (IOP)

1.4.3 Types of Glaucoma:

There are various types of Glaucoma which are stated as below [13]:

1. Primary Open-Angle Glaucoma
2. Normal Tension Glaucoma
3. Angle-Closure Glaucoma
4. Pigmentary Glaucoma
5. Exfoliation Syndrome
6. Trauma-Related Glaucoma

Out of the different types of glaucoma, only first three types are discussed as they are the commonly caused Glaucoma worldwide.

1. **Primary Open-Angle Glaucoma (POAG):** There are no side effects related with POAG. The tension inside the eye gradually rises and the cornea adjusts without swelling. But the condition of the eye worsens with the swelling of cornea. This is not the condition so this illness normally goes unobserved. It is effort less and the effected person does not understand that his vision is slowly vanishing till the last stage of disease. The harm is irreversible till the eyesight is lost.

   In POAG, there is no unique variation from the norm of the trabecular meshwork. It is believed that something is wrong with the volume of the cells in the trabecular meshwork to do their ordinary capacity, or there might be less cells present as a characteristic aftereffect of getting more seasoned. POAG is a chronic disease having no cure at present but can be decelerated by treatment.
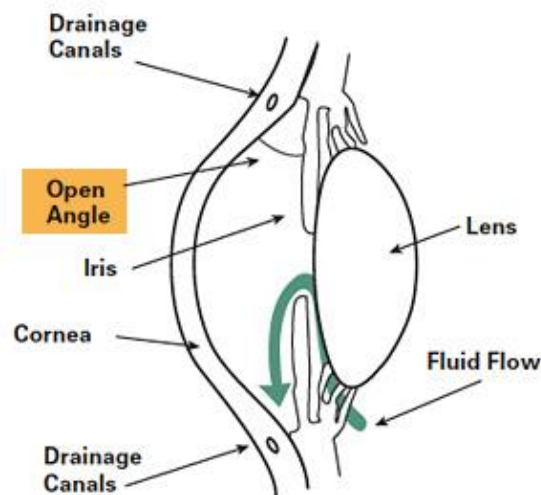
Figure 1.11: Primary Open-Angle Glaucoma [5]

2. **Normal Tension Glaucoma:** It is also termed as low-pressure glaucoma and explained by active optic nerve harm and visual field misfortune with a measurably ordinary IOP. Typical pressure glaucoma is believed to be connected to lack of blood stream to the optic nerve which prompts demise of the cells that convey motivations from the retina to the mind. [13].

3. **Angle Closure Glaucoma:** Half a million of people is affected by this disease in US. The people who are affected with this disease have the anterior chamber whose size is smaller than average. The angle of the eye is situated between the peripheral iris and peripheral cornea which contains a trabecular meshwork. The trabecular meshwork serves as the filter for the aqueous humor. The finer the angle, the nearer the iris is to

the trabecular meshwork. When the angle is 45 degrees and below then the person is diagnosed with angle closure glaucoma.
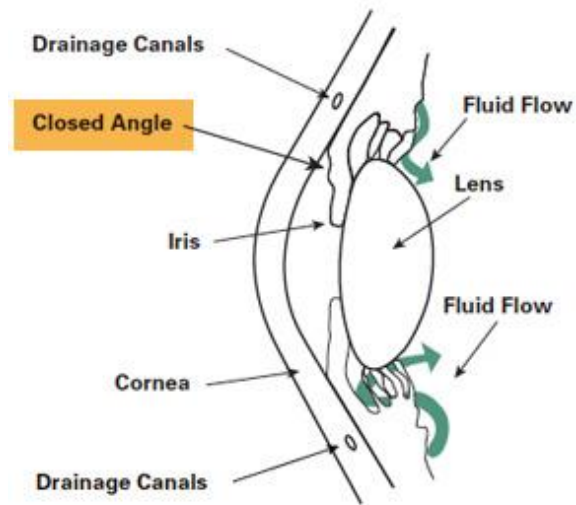
Figure 1.12: Angle-Closure Glaucoma [5]

In this chapter, we have studied details of human eye and disease related to eye which affect the vision of the eye. Glaucoma is discussed in more detail as it is the second most reason for the blindness across the world. Early detection and treatment of this disease can prevent the vision loss in the person. In Chapter-2, different methods proposed by different authors for the detection of Glaucoma at early stage are discussed and comparison table is made. Chapter-3 tells about the general methodology used for the detection of Glaucoma. Chapter-4 discusses the implemented method using EWT Transforms for the Glaucoma detection. Chapter-5 concludes the work done and tell us about the limitations and future scope of this research.

CHAPTER-2

LITERATURE REVIEW

In this section, various methods proposed by different authors has been discussed.

1) Agarwal *et al*. [14], had proposed an adaptive thresholding method in which features like mean, standard deviation to segment the optic disk to optic cup are extracted from the images which make this method independent of the noise and image quality. This method gives the 90% accuracy.

2) Pruthi *et al.* [15] had given a method for Glaucoma detection by the cup to disk ratio (CDR) analysis. The methodology suggested by the author consists of 6 stages involving: pre-processing the data by illuminance correction, blood vessel removal. ROI extraction after pre-processing the images, followed by the feature extraction technique where optic disc extraction, optic cup extraction, morphological operations, ellipse fitting are some of the steps. The method discussed gives 98.12% accuracy.

3) Virk *et al.* [16] suggested a simple method i.e. CDR determination for the screening of Glaucoma. The author had specified one threshold value for CDR i.e. 0.5. If the CDR is greater than 0.5 then one can be suspected with Glaucoma. It gives 95% accuracy. The detection rate for CDR determination was 80% which needs more improvement.

4) Gopalkrishnan *et al.* [17] proposed a technique to segment the Optic Disc (OD) Segmentation using Circular Hough Transform and Curve Fitting boundary from the retinal images. It had used a circular Hough transform for the detection of Glaucoma in early stage. But the accuracy of the method was 68%. This method can be extended and improved using the OCT images.

5) Ayub *et al.* [18] had proposed a method of Optic Disc and Cup Segmentation using K mean Clustering. Since for this method, firstly, ROI was being extracted which was further followed by the pre-processing technique which improves the image quality. In this techniques ellipse fitting was used for smoothening the boundary of OC and OD. Further using these techniques CDR was calculated and used for the early detection of Glaucoma. The advanced process gives the accuracy of 92% for Glaucoma detection.

6) Sakthivel *et al.* [19], suggested a technique for glaucoma detection using the Histogram Features Detection Technique. In these method different algorithms like Local Binary

pattern (LBP) and Daugman's algorithm had been used for the feature extraction of the data. Histogram was performed for both magnitudes as well as phase components in the data. For the classification of the data, Euclidean distance between the feature vectors has been analyzed.

7) Kolar *et al*. [20] suggested a method depends on the fractal description which was followed by the classification process. For fractal dimensions estimation, two methods were given which explainsdifferent image information. Retinal nerve fibers was analyzed which were taken from the fundus color images. As losses in the retinal nerve fiber was the symptom of the glaucomatous eye, so it can be used as one of the feature for the detection of the Glaucoma.

8) Acharya *et al*. [21] presented a technique in which Glaucoma can be detected using combination of Higher Order Spectra (HOS) and texture features obtained from the retinal digital fundus images. These features after z-score normalization are fed to random-forest classifier which can be used clinically for detecting glaucoma accurately with the accuracy of 91%.

9) Acharya *et al.* [22] proposed a method in which Gabor transform was used where various features were extracted from the retinal fundus images. These features are mean, variance, skewness, kurtosis, energy and Shannon entropies. PCA was done to reduce the dimensionality of the features. This method gives the 93.1% accuracy. Author had also proposed a GRI which was developed using principal components to classify the 2 classes using 1 number only. This will reduce the complexity and reduce the classification time for the Glaucoma images.

10) Shishir *et al*.[23] developed a method for the detection of Glaucoma which consists of Empirical Wavelet Transform (EWT) using fundus images. EWT components were used to extract the correntropy features which were ranked depending upon t-value feature selection algorithm. 98.33% accuracy was obtained using Least SVM which decrease to 96.67% if 3 fold and 10-fold cross validation was used.

11) Krishnan *et al*.[24] proposed a method in which they used the texture features for the detection of Glaucoma. In this method, classification accuracy of 91.67% was obtained using the SVM classifier.

12) Nyul *et al.* [25] suggested a method in which author followed three steps process i.e. pre-processing, feature extraction and classification for the detection of the Glaucoma. In pre-processing, different methods i.e. illumination correction, vessel improvement

and normalization were employed. Different features were extracted using generic method and these features were classified using SVM classifier in which classification accuracy comes to be 80%.

13) Bock *et al*. [26] presented a method for the detection which used a standard pattern recognition pipeline with two stage classification. In this method, features extracted were termed as appearance based features which include pixel intensity values, spectral based, texture and histogram model values. In this approach of Glaucoma detection 86% accuracy was obtained using SVM classifier.

14) Mookiah *et al*. [27] presented an automatic detection method for Glaucoma using the HOS and DWT features. These features with SVM classifier were able to detect Glaucoma with an accuracy of 95%. This method can be employed for the earlier detection of glaucoma.

15) Dua *et al*.[28] presented a method in which texture features like energy signatures were used as the exact and efficient approach for the detection of Glaucoma. In this method, author extracted energy signatures present within the images using 2D DWT feature extraction technique and different feature ranking and feature selection algorithms were followed. 93% accuracy was obtained using different classifiers like SVM and naïve Bayes classifier with tenfold validation.

16) Beaula *et al*. [29] proposed a methodology for the early detection of the Glaucoma using empirical wavelet transform. In this method, author extracted the correntropy features from the EWT components obtained in the feature extraction process. These features were selected using t-test algorithm. 95% Classification accuracy was obtained with the SVM classifier.

17) Patil *et al*. [30] proposed a methodology in which the diagnosis was done using the CDR method. In this method, the super pixel classification on the basis of the cup to disc ratio was done to identify Glaucoma. Color contrast improvement and image filtration were the preprocessing techniques used with the segmentation process for the glaucoma detection.

18) Dey *et al*. [31] suggested automated glaucoma selection using support vector classification. In this method, images pre-processing techniques like noise removal and contrast enhancement were used. Principal Component Analysis (PCA) method was employed for feature extraction and SVM method for image classification. This method after cross validation gave accuracy rate 96%

19) Singh *et al.*[32] suggested a method for glaucoma detection. This method employs various steps for the diagnosis which are pre-processing, feature extraction and classification. 97% accuracy was obtained when used with SVM classifier.

Table 2. 1: Comparison of the methods used for the detection of Glaucoma

S.No.	Authors	Methods given by authors	Images Number	Features extracted	Classifier	Accuracy (%)
1)	Agarwal *et al.* [14]	Adaptive thresholding	110 images	CDR, mean, standard deviation	Thresholding	90%
2)	Pruthi *et al* .[15]	CDR Calculation	10normal/10 glaucoma	CDR	SVM	98.12%
3)	Virk *et al.* [16]	CDR Determination	50 images	CDR	Thresholding	95%
4)	Gopalkrishan *et al.*[17]	Segment OD boundary	200 images	CDR	Least square minimization	68%
5)	Ayub *et al.* [18]	Optic disc and Cup segmentation using K-mean clustering	100 images	CDR	K-mean Clustering	92%
6)	Sakthivel *et al.* [19]	Histogram	44 images	LBF	Euclidean Distance	95.45%
7)	Kolar *et al.* [20]	Fractal Dimensions	30 images	Fractal and power	SVM	74%

16

				spectral features		
8)	Acharya *et al.*[21]	Diagnosis using texture and HOS feature	60 images	HOS and texture	Random-forest	91%
9)	Acharya *et al.* [22]	Using Gabor Transformations	510 images	Gabor features	SVM	93.1%
10)	Shishir *et al.* [23]	Using EWT and Correntropy features	505 images (Public Database) and 60 images (Private database)	Correntropy features	LS-SVM	98.33%
11)	Krishnan *et al.* [24]	Detection using texture , DWT energy and HOS features	60 images	HOS and energy features	SVM	91.67%
12)	Nyul *et al.* [25]	Glaucoma detection	NA	PCA	SVM	80%
13)	Bock *et al.* [26]	Texture analysis for detection	NA	Pixel intensity values, FFT coefficients	SVM	86%
14)	Mookiah *et al.* [27]	NA	NA	HOS and wavelet	SVM	95%
15)	Dua *et al.*[28]	Detection using texture features	60 images	Energy signatures	SVM	93.33%

16)	Beaula *et al.* [29]	Detection using texture features	NA	Correntropy	SVM	74%
17)	Patil *et al.* [30]	Using CDR	NA	CDR	SVM	NA
18)	Dey *et al.* [31]	NA	NA	NA	SVM	96%
19)	Singh *et al.* [32]	Detection of glaucoma	220 images	Red, Green and Blue values	SVM	97%

This chapter discusses and compares different methods available for the detection of glaucoma using fundus images. In the Chapter-3, general methodology used in the detection of glaucoma is discussed in detail.

CHAPTER-3

METHODOLOGY

The general flow diagram for the detection process of glaucoma [33] is shown in Figure 3.1. In this section, different steps involved in the detection of Glaucoma are discussed.
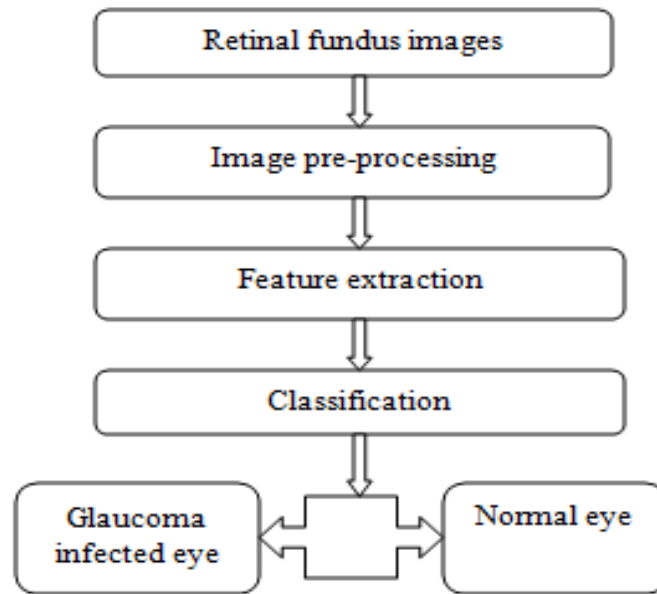
Figure 3. 1: General flow diagram for the Glaucoma detection

3.1 COLLECTION OF DATA

For the implementation of CAD system, data is collected from different databases which can be either public or private. In the Glaucoma detection process, there are basically two types of images available that can be used for the detection. These are optical coherence tomography and retinal fundus images.

Optical Coherence Tomography (OCT) [34]: It is a technique in which images are obtained from the optical scattering media. It uses coherence light to capture the micrometer resolution, 2D and 3D images.
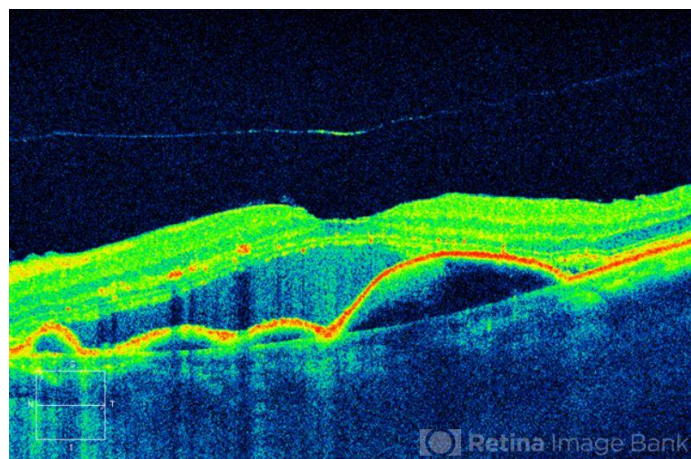
Figure 3. 2: OCT images [35]

Retinal Fundus Images [36]: It involves taking a photograph of fundus of the eye. For the fundus photography, there are specialized fundus cameras available that consist of the convoluted microscope which is attached to a flash enabled camera. The retina (central and peripheral retina), macula and optic disc are the main structures which can be imagined on the fundus photo. It can be achieved with colored filters or using specialized dyes (fluorescein and indocyanine green).

Figure 3. 3: Retinal fundus image [37]

Different databases are available online containing fundus images and OCT images. Following is the list of few databases available.

1. **High Resolution Fundus (HRF) Database [38]**: It is a public database established by a research group for the support of comparative study on automatic segmentation algorithm on retinal fundus images. It contains 15 fundus images of healthy person, 15 fundus images of patient suffering from the Diabetic retinopathy and 15 fundus images of the patients suffering from Glaucoma.

2. **ACHIKO-K Database [39]**: It contains 258 of manually recorded retinal images with the information of their clinical diagnosis. The images available in this database are taken from glaucoma patients and contain rich information of glaucoma pathological symptoms e.g. optic cup scoring, optic nerve drusen and hemorrhage.

3. **Digital Images for Optic Nerve Segmentation Database (DRIONS –DB) [40]:** There are 110 color fundus images taken by the color fundus camera centered at optic nerve hypoplasia (ONH) and store in the slide format. These images are digitized using a HP-Photomart-S20 high resolution manner, stored in RGB format. Size of each image pixel is 8bits\pixel at a resolution of 600x400.

4. **RIM-ONE [41]:** It is composed of 169 ONH images which are obtained from the 169 full fundus images of different subjects. It is developed in order to be reference for the design of optic nerve segmentation algorithm.

5. **Medical Image Analysis Group[42]**: There are 255 fundus images of healthy person and 250 fundus images of the patient suffering from Glaucoma. It is available online at http://medimrg.webs.ull.es/. Format at which these fundus images are available are 24-bit JPEG at different resolution.

Table 3.1 show the different database used for detection of Glaucoma in various available methods discussed in Chapter-2.

Table 3.1: Summary of different databases used in the detection of Glaucoma

S.No.	Authors	No. of Images	Database
1)	Agarwal *et al* [13]	110 images	Local database (Venue Eye Research Centre, New Delhi)
2)	Pruthi*et al* [14]	10normal/10	

		Glaucoma	
3)	Virk *et al*[15]	50 images	Local Physician
4)	Gopalkrishan *et al* [16]	200 images	RIGA
5)	Ayub *et al* [17]	100 images	Local-database (Armed forces institute of ophthalmology)
6)	Sakthivel *et al* [18]	44 images	Local database (Aravind Eye Hospital, Madurai, India.)
7)	Kolar *etal* [19]	30 images	NA
8)	Acharya *et al*.[20]	60 images	Local database (Kasturba Medical College, Manipal, India)
9)	Acharya *et al*[21]	510 images	Local database (Kasturba Medical College, Manipal, India)
10)	Shishir *etal* [22]	505 images (Public Database) and 60 images (Private database)	http://medimrg.webs.ull.es/. (Public Database) Kasturba Medical College, Manipal, India.(Private Database)
11)	Krishnan *et al* [23]	60 images	Kasturba Medical College, Manipal, India.(Private Database)
12)	Nyul *et al* [24]	NA	Erlangan Glaucoma Registry
13)	Bock *et al* [25]	NA	NA
14)	Mookiah *et al* [26]	NA	NA
15)	Dua *et al* [27]	60 images	Kasturba Medical College, Manipal, India.(Private Database)

16)	Beaula *et al* [28]	NA	NA
17)	Patil *et al* [29]	NA	Atharva Eye Care Hospital, Pune
18)	Dey *et al* [30]	NA	NA
19)	Singh *et al* [31]	220 images	http://www.tf.fau.de/ (public database) and TechnischeFakultat (private database)

3.1 PRE-PROCESSING

Pre-processing is a procedure which employs various operations on the images at the lowest level of abstraction. The main purpose of pre-processing is an enhancement of the image data by suppressing the reluctant alterations and improves important image features used in further processing, while geometric transformation of images like scaling etc. are categorized in preprocessing methods [43].

Following are the number of the techniques available for the pre-processing:

1. Data Cleaning
2. Data integration
3. Data Transformation
4. Data reduction

1. **Data Cleaning:** Data cleaning, while identifying outliers and improving the variation of data aims to fill the missing values and remove the noise by various methods. Binning method improves the data by negotiating the neighboring values. Local smoothing is performed, as the effect of smoothing is larger because of its larger width. It is used as discretization technique. Regression is a technique in which data is levelled by fitting it into a function. Linear Regression is a method involving detection of one attribute out of two so that one can be used for prediction of other. Clustering is a method in which similar data is organized into groups and used for the detection of the outliners.

2. **Data Integration & Transformation:** Data Integration is the converging of data from various data stores. Correlation analysis can be used for the detection of redundancy and also be detected at the tuple level. Due to difference in representation there is conflict in

the detection and resolution of data value. The data is modified into the forms that are suitable for mining.

a) Smoothing is a process that help in removal of noise from the data including binning, regression and clustering.

b) Aggregation is the process that is used for construction of data cubes and in the analysis of data at various granularities.

c) By using the hierarchies, low level data or raw data is replaced by higher level is the generalization of data.

d) When in a small specified range attributes of data are scaled is normalization.

  i. Max – Min Normalization performs linear conversion of original data.

$$z = \frac{x - min(x)}{max(x) - min(x)} \qquad (1)$$

  ii. Z – Score Normalization is based on mean (μ) and standard deviation (σ) of the data.

$$z = \frac{x - \mu}{\sigma} \qquad (2)$$

  iii. Normalization by decimal scaling is done by rounding-off the decimal point to the nearest attribute value.

$$v' = \frac{v}{10^j} \qquad (3)$$

3. **Data Reduction:** Data reduction is smaller in volume that can be applied to obtain a reduced representation of the data. Data Cube Aggregation is a series of operations that are applied to the data for the data cube construction. When inappropriate, inadequately redundant attributes or dimensions are detected or separated is termed as attribute subset selection. Dimensionality reduction is a method in which encoding mechanisms are used for the reduction of the data size. When the data is exchanged or its alternative is estimated is termed as numeriosity reduction. Here smaller data representations like parametric modes and non-parametric procedures like clustering, sampling and use of histograms is done.

Table 3.2 summarizes different pre-processing methods used in the detection of Glaucoma. These methods are discussed in Chapter-2.

Table 3.2: Summary of pre-processing methods used in the detection process.

S.No.	Authors	Pre-processing techniques
1)	Agarwal *et al* [13]	Red ,Green and Blue channel extraction
2)	Pruthi*et al* [14]	Anisotropic diffusion filter
3)	Virk*et al*[15]	NA
4)	Gopalkrishan*et al* [16]	Localized Gaussian Smoothing
5)	Ayub*et al* [17]	Morphological operations, Equalization , Color Enhancement
6)	Sakthivel*et al* [18]	Gabor filter
7)	Kolar *etal* [19]	Fractal Analysis
8)	Acharya *et al*.[20]	Radon Transform , Histogram Equalization
9)	Acharya*et al*[21]	Histogram Equalization
10)	Shishir *etal* [22]	Red ,Green and Blue channel extraction
11)	Krishnan *et al* [23]	Histogram equalization , Radon transformation
12)	Nyul *et al* [24]	Illumination correction, Vessel removal, Papilla normalization
13)	Bock *et al* [25]	Normalization
14)	Mookiah *et al* [26]	NA
15)	Dua *et al* [27]	Histogram equalization
16)	Beaula *et al* [28]	Red ,Green and Blue channel extraction
17)	Patil *et al* [29]	Histogram equalization
18)	Dey *et al* [30]	NA
19)	Singh *et al* [31]	NA

3.2 FEATURE EXTRACTION MODULE

Feature extraction is a set of operation use for the conversion of visual extractable and non-extractable features into respective mathematical terms. Detection of basic features like spot, edge, ripple and wave is done in techniques used in feature extraction methods in the normal as well as gray level images[44-47]. These mathematical terms based on shape are termed known as morphological features and if they are based on intensity distribution then termed as texture features. The feature extraction is further classified into two types Statistical Features and Texture Features

a) **Statistical Features**: It is a technique applied for extraction of texture features which are based on gray level intensities of an ultrasound image is termed as statistical methods.

b) **Transform Domain Features:** By using various multiple resolution schemes, the transform domain is used for feature extraction over several scales. To analyze the texture of image, it is logical to compute texture feature in the transform domain as human visual system processes image[48]. The schemes of transform domain are:

    i.   Wavelet Packet Transform (WPT)

    ii.   Gabor Wavelet Transform (GWT)

    iii.   Fourier Power Spectrum (FPS)

    iv.   Empirical Wavelet Transform (EWT)

i.   **WPT:** It is a wavelet transform in which the wavelets are sampled in packets. In this transform frequency as well as location information is calculated which is its advantage over the Fourier transform. There are enormous number of applications in Science, Mathematics and Engineering. It is used for signal coding for signifying the signal in most excessive form.

ii.   **GWT**: Gabor wavelets are the mathematical tools used to find the optimal solution in the analysis of any mathematical function. It is mostly utilized in the analysis of the signal. The applications of GWT generally are tracking of objects, detection of edges and extraction of texture features. Gabor wavelets transformation provide solution to various application issues like Image Compression, Filter Design and Edge Detection.

iii. **FPS Features**: In this process, from Every ROI two spectral features are calculated by Discrete Fourier Transform. These spectral features are Radial Sum and Angular Sum

iv. **EWT:** EWT [49-52] is a recently proposed procedure to adaptively identify the different modes of the signal and consequently build the empirical wavelets to characterize the signal by different modes detected. Here frequency spectrum of the processed signal is detected on the basis of which modes are constructed. Modes can be referred as the major components of the signal which characterize the signal fully. The features which are extracted from the decomposed images are termed as Correntropy

The main purpose of EWT method is signal decomposition [50]. EWT definition is based on the choice of the support of Fourier domain because they depend on the analyzed signal. EWT consists of two main steps:

a) Detection of the Fourier boundaries and build the corresponding wavelet based on these boundaries.

b) Filter the image from the obtained the filter bank to get the components.

In EWT, the Fourier spectrum range 0 to π is divided into M number of parts where divided parts are termed as segment. Limit of each segment is given by ω_m, ranging from $\omega_0 = 0$ and $\omega_m = \pi$. The transition phase T_m depends upon ω_m which has width of $2f_m$, where $f_m = a\,\omega_m$ for $0 < a < 1$[52]. Empirical wavelets are defined on each neighboring section by the constructed filter bank. The empirical scaling function $\xi_m(X)$ and the empirical wavelets $\varsigma_m(X)$ can be described by equation 3 and 4 [53].

$$\xi_m(X) = \begin{cases} 1, & if\,|X| \leq (1-a)w_m \\ \cos\left[\dfrac{\Pi}{2}Y(a-w_m)\right], & if\,(1-a)w_m \leq |X| \leq (1+a)w_m \\ 0, & otherwise \end{cases}$$

(3)

$$\varsigma_m(X) = \begin{cases} 1 & if\,(1+a)\omega_m \leq |X| \leq (1-a)\omega_{m+1} \\ \cos[\dfrac{\pi}{2}Y(a,\omega_{m+1})] & if\,(1-a)\omega_{m+1} \leq |X| \leq (1+a)\omega_{m+1} \\ \sin\left[\dfrac{\pi}{2}Y(a,\omega_m)\right] & if\,(1-a)\omega_m \leq |X| \leq (1+a)\omega_{m+1} \\ 0 & otherwise \end{cases}$$

(4)

where $Y(a, \omega_m)$ and $Y(a, \omega_{m+1})$ are defined by equation (5) and (6) respectively.

$$Y(a, \omega_m)=F\left(\frac{1}{2a\omega_m}(|X| - (1 - a)\omega_m)\right) \tag{5}$$

$$Y(a, \omega_{m+1})= F\left(\frac{1}{2a\omega_{m+1}}(|X| - (1 - a)\omega_{m+1})\right) \tag{6}$$

Fourier Boundaries Detection

The technique recommended for the recognition of Fourier boundaries is established on the detection of local maxima in the spectrum magnitude assuming that is composed of appropriately separated modes. [54]Basically there are mainly two ways for the detection process:

a) Detection of local maxima method by finding the lowest minima or by global trend removing.

b) Fine to Coarse Histogram Segmentation Algorithm

Types of EWT: EWT is classified further on the basis of dimensions which are [54-55] Empirical Wavelet Transform 1 Dimension (EWT 1D) and Empirical Wavelet Transform 2 Dimension (EWT 2D)

i. **EWT 1D:** The basic idea is the construction of significant filter bank of M wavelet filters ($M - 1$) band pass filters and one low pass filters) which is based on Fourier boundaries obtained from the analyzed signal.

ii. **EWT 2D**: It is further classified into four parts are EWT 2D Curvelet, EWT 2D Littlewood Paley, EWT 2D Ridgelet and EWT 2D Tensor.

a) **EWT 2D Tensor**: 1D EWT is applied on the signals but to apply it to images 1D EWT is extended by tensor approach as done 2D DWT. In 1D EWT, idea was that rows and columns are considered independent of each other which results in various sets of filters explained on different Fourier boundaries. But this leads discontinuity in the filter bank for every row and column different spectral information is obtained on same scale. To solve this problem, a tensor approach in the method is proposed to use same filter bank for processing of all rows and second filter bank for processing all columns. The results

obtained are the decomposed images after processing of rows and columns from the constructed filter.

b) **EWT 2D Curvelet:** Cand`es introduced the concept of the curvelet transform. The basic idea behind is to construct a filter bank in the Fourier domain where each filter has its boundaries located on a polar wedge. A decomposition is used on the partition of the Fourier plane i.e. low frequency are located on a disk centered at the zero frequency and every scale is defined on the concentric annuli. Here empirical extension in this concept will detect both the scales as well as angles which corresponding to each polar edge.

Let us assume that M_s as the number of scales and M_ϕ as the number of angels which are detected. In the detection process, set of scaling boundaries and a set of angular boundaries are calculated first. For the detection of the standard curvelet, radial window in the Fourier domain is defined as X_a where a is the scale indices. X_a can be defined on 2 conditions i.e.

When $a \neq M_s\text{-}1$

$$X_a(z)$$

$$= \begin{cases} 1 & (1+\tau)Z^a \leq |Z| \leq (1-\tau)Z^{a+1} \\ cos[\frac{\pi}{2}\alpha\left(\frac{1}{2\tau z^{a+1}}(|Z|-(1-\tau)Z^{a+1})\right] & if\,(1-\tau)Z^{a+1} \leq |Z| \leq (1+\tau)Z^{a+1} \\ sin\left[\frac{\pi}{2}\alpha\left(\frac{1}{2\tau Z^a}(|Z|-(1-\tau)Z^a)\right)\right] & if\,(1-\tau)Z^a \leq |Z| \leq (1+\tau)Z^a \\ 0 & ,otherwise \end{cases}$$

$$(7)$$

When $a = M_s\text{-}1$

$$X_{Ms-1}(Z)$$

$$= \begin{cases} 1, & if\,(1+\tau)Z^{Ms-1} \leq |Z| \\ sin[\frac{\Pi}{2}\alpha\left(\frac{1}{2\tau Z^{Ms-1}}(|Z|-(1-\tau)Z^{Ms-1})\right] & if\,(1-\tau)Z^{Ms-1} \leq |Z| \leq (1+\tau)Z^{Ms-1} \\ 0, & otherwise \end{cases}$$

$$(8)$$

Then, the filter bank is designed based on the concept that angular window constructed from the polar wedge is dependent on a.

c) **EWT 2D Littlewood Paley:** The classic 2D Littlewood-Paley wavelet transform corresponds to filter images with 2D wavelets defined in the Fourier domain on annuli boundaries which are centrally originated. The outer and inner radius of these boundaries depend upon the decomposition of the Fourier plane. In this approach, radius of each annuli is detected. The best method for the detection is to consider Fourier plane in polar coordinates. The 2D empirical littlewood-paley transform of an input image y is given by

$$W_y^{elp}(n,a) = X_2^*(X_2(y)(Z)\overline{X_2(\phi_n)(Z)}) \tag{9}$$

where $W_y^{elp}(n,a)$ is the 2D littlewood-paley components, X_2^* and X_2 are the 2D Fourier transform and its inverse and ϕ_n and Z are the parameters of the filter.

d) **EWT 2D Ridgelet:** Cand`es and Donoho [7, 8, 16] introduced the concept of ridgelet transform and it was the first directional 2D wavelet type transform. Ridgelet transform is same as littlewood-paley transform. Fourier boundaries are detected on an average spectrum which is obtained from the Pseudo-polar FFT. The ridgelet empiral transform is defined as:

$$W_y^{er} = W_y^e \left(X_{1,Z}^* \left(X_p(y) \right) \right) \tag{10}$$

where W_y^e is the 1D ridgelet transform, W_y^{er} is the 2D ridgelet transform, $X_{1,Z}^*$ is the 2D Fourier transform inverse and $X_p(y)$ is the pseudo-polar FFT.

Correntropy features are extracted from the EWT decomposed components as it is calculates the correlation in the non-linear domain. It can be used for the detection of non-linear outliers with any difficulty. It also conserves both arithmetical and sequential information.

Correntropy:

The basic idea of correntropy is a similarity measure between two arbitrary random variables A and B having the same dimensions. [56-59]. It measures correlation in nonlinear domain. Correntropy is a kernel based measure. It can be used for the measurement of distribution of texture in the decomposed image components. Correntropy is also useful for the diagnoses of coronary artery disease. Correntropy is defined as

$$V(A,B) = E[k(A,B)] = \int k(a,b)dF_{AB}(a,b)$$

Where

V denotes the correntropy

E [] denotes the mathematic exception

$F_{AB}(a, b)$ denotes the joint distribution function of the A9 and B

K () denotes the shift variance Mercer kernel

As in correntropy, concept of kernel is used so most popular kernel used in the procedure is the Gaussian kernel. Gaussian kernel has the kernel width $\sigma > 0$. General equation for the Gaussian kernel is given as:

$$k_\sigma(a, b) = \frac{1}{\sqrt{2\pi\sigma}} exp \left[\frac{||a-b||^2}{2\sigma^2} \right] \tag{12}$$

When the joint distribution of A and B is unknown and only a finite *M* no. of samples $\{(a_i, b_i)\}_{i=1}^N$ are given. The correntropy estimator of samples $\widehat{V_N}(A, B)$ can be defined and calculated as follows

$$\widehat{V_N}(A, B) = \frac{1}{N} \sum_{i=1}^N k_\sigma(a_i, b_i) = \frac{1}{N\sigma\sqrt{2\pi}} \sum_{i=1}^N exp[\frac{-(a_i, b_i)^2}{2\sigma^2}] \tag{13}$$

The number of correntropy features depends on the kernel value. For the calculation of correntropy, value of *N* is taken as 1.Correntropy is strictly related to the comparison between *A* and *B* and both the random variables are similar to each other than the difference between *A* and *B* have the large of value of correntropy.

3.4 CLASSIFICATION MODULE: The procedure towards gathering the testing data into the comparing classes is known as classification of dataset. It is arranged into the following: are Supervised Classification and Unsupervised Classification.

1. Supervised Classification: It is defined when the classes are previously defined for the training sets. [60].
2. Unsupervised Classification: When there are undefined classes in the training set then the classification is termed as the unsupervised techniques.

Different classifiers like k-NN, PNN, SVM, SSVM and ANN are engaged to classify the unknown testing cases of numerous ultrasonic classes that are based on the training instances.

1. ***k*-Nearest Neighbor**: It depends on the idea of evaluating the class of an unspecified form of its neighbors. The fundamental principle is the presumption of the feature vector lying near each different having similar class. In the training dataset while looking among k-nearest the class of an unidentified example is chosen. The key advantage of k-NN is its capacity to deal with various class issues and it is additionally strong to the noisy data problem as it averages the *k*-nearest neighbors of the data [61-63]. The estimation of k is significant factor in *k*-NN classifier as classification performance of *k*-NN relies upon the value of *k*.
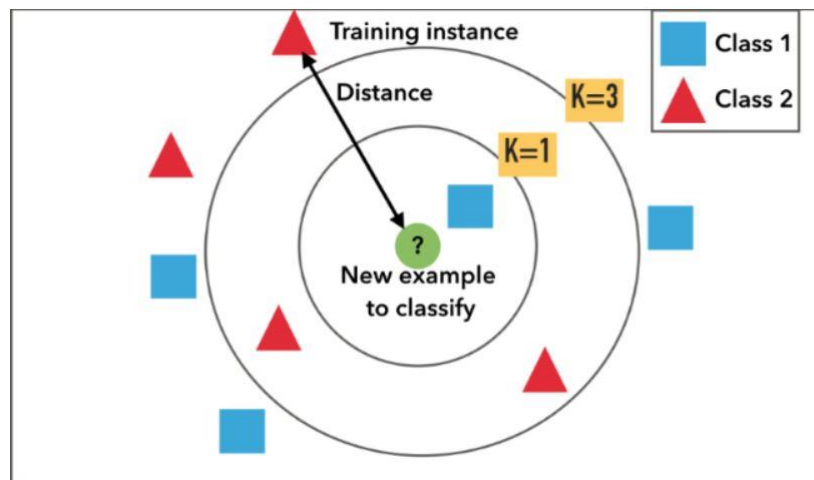
Figure 3. 4: *k*-nearest neighbor estimation[62]

2. **Artificial Neural Network**: The ANN are the computational model which are depends on the substantial grouping of simple neural network units. Each neural unit is associated with numerous different units and links which can improve the activation state of adjoining neural units. By the use of summation function, each neural unit can be analyzed. The ANN is group of numerous artificial neurons that are connected together according to a detailed architecture of network. Its principal objective is to change inputs into significant outputs. The ANN is used to accomplish the objective to controlling the development of a robot created on self- perception and other data. These frameworks are self-learning and prepared and work in the zones where the feature identification is hard to extract [64-66].
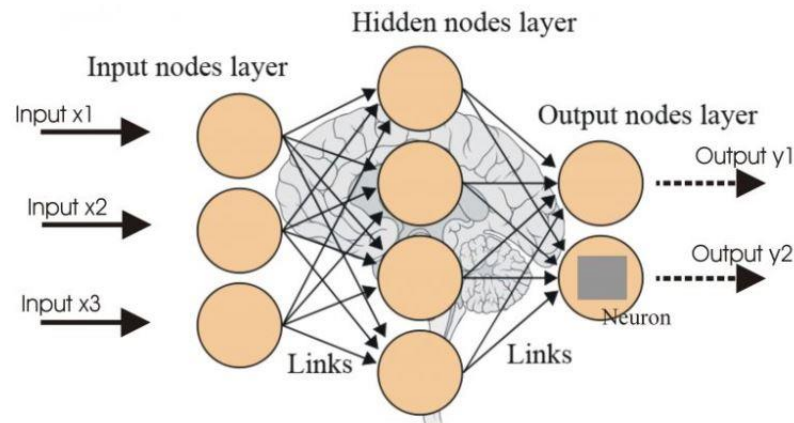
Figure 3. 5: Basic structure of ANN [64]

3. **Support Vector Machine**: The SVM classifier goes under the class of regulated learning machine and chips away at the premise of number-crunching idea and factual hypothesis. SVM classifier can characterize both straight and non-direct order. With the assistance of the accessible preparing information it makes the hyper plane between the classes which brings about great division accomplishment instinctively however the sets that are accessible to separate are not directly distinguishable in the space. In non-direct order module, the information is mapped from input space to higher dimensional element space by utilizing the info information which is mapped into the part work [65]. The Gaussian spiral premise work has been utilized for grouping of the information..
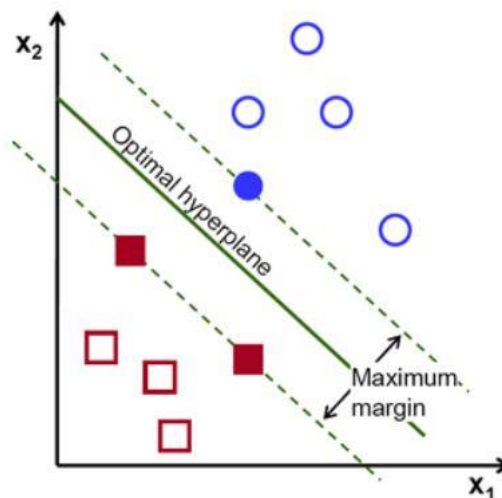
Figure 3. 6: Estimation of SVM [65]

4. **Smooth Support Vector Machine**: It is the innovative and enhanced form of SVM classifier. The motivation behind SSVM classifier is to attain unconstraint smoothing and unconstrained optimization reformulation which could not achieved by utilizing SVM classifier as it is related to the conventional quadratic program [67]. In execution, the ten-fold cross validation is performed on training data for each grouping. The ideal estimation of C is given by the method of grid search in parameter space for which training accuracy is maximum.
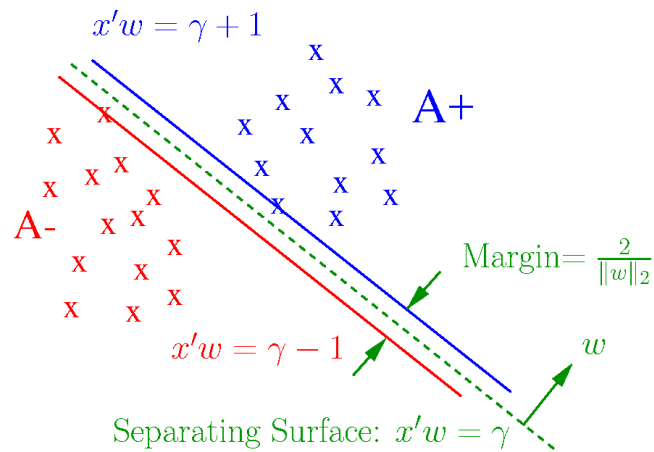
Figure 3. 7: Distribution in SSVM[67]

5. **Least Square Support Vector Machine:** Least square SVM is a controlled learning technique which is used for the analyzation of data and pattern recognition used in the used in the regression analysis and classification modules. It was proposed by Suykens and Vandewalle. They are categorized as kernel based learning method. This technique solves the linear equations rather than convex quadratic programming problem that are used in classic SVM. [68]
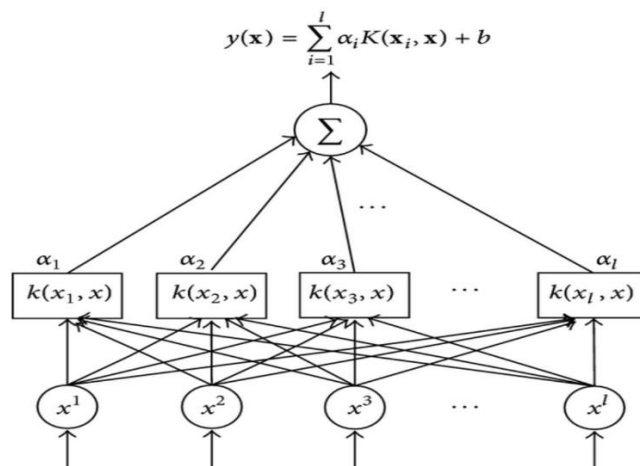
Figure 3. 8: Structure of LS-SVM [68]

6. **Maximum Likelihood Classifier:** It is the most well-known technique among the available techniques available in classification module in remote sensing where a pixel with the maximum likelihood is categorized into the equivalent class.[68] The probability Lk is defined as the subsequent likelihood of a pixel having a place with to class k.
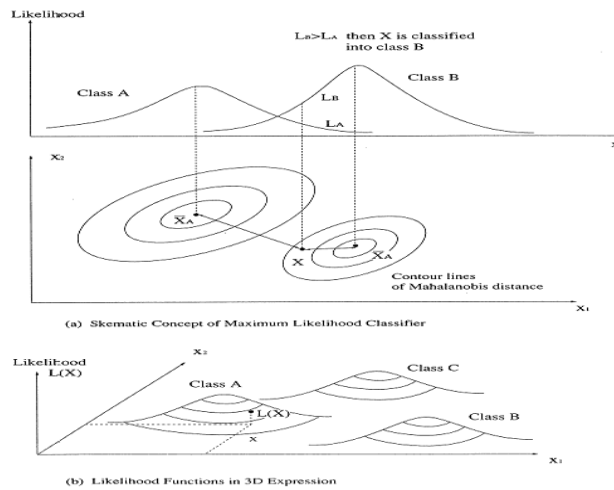
Figure 3. 9: Distribution in Maximum likelihood classifier [68]

CHAPTER-4

COORENTROPY FEATURE AND EMPIRICAL WAVELET TRANSFORM BASED GLAUCOMA CLASSIFICATION FROM FUNDUS IMAGE

Many transform methods like Discrete Wavelet Transform (DWT), Fourier Transform can be used as the feature extraction technique in the Glaucoma detection. But we have used EWT technique as the feature extraction. EWT is better than other wavelet methods because it uses no predefined function as used in DWT and Fourier method. In EWT, the basis function used in the process is generated accordingly to the information present in the data (signal or image).

The method implemented for the recognition of Glaucoma is based on the EWT and correntrophy features. These features are acquired from the EWT decomposed images as EWT decomposes the image into several frequency bands based on the information present in the image. These features are further normalized and ranked on the basis of student t-test criteria. SVM is used as a classifier. Five cross validation approach is used to detect Glaucoma at early stage. These steps are already discussed in detail in Chapter-3. This chapter discusses the algorithm involved in the method for the Glaucoma detection process. Figure 4.1 shows the flow diagram involved in the implementation of this detection.

Step 1: Data Collection:

For the implementation of this method, retinal fundus images are used. These images are collected from the Medical Image Analysis Group discussed in Chapter 3. We have used 50 normal and 50 glaucoma images out of total 455 images available in the database. Figure 4.2 shows the images collected from the database.

Features	Normal	Glaucoma	t value
CE_{12}	2.1386	-2.0066	6.021
CE_{16}	2.124	-2.1372	3.871

Correntropy calculation and Feature selection (student t-test)

Feature extraction (Empirical Wavelet Transform)

Classification using SVM classifier

GLAUCOMA EYE

NORMAL EYE

Data collection

Pre-processing technique
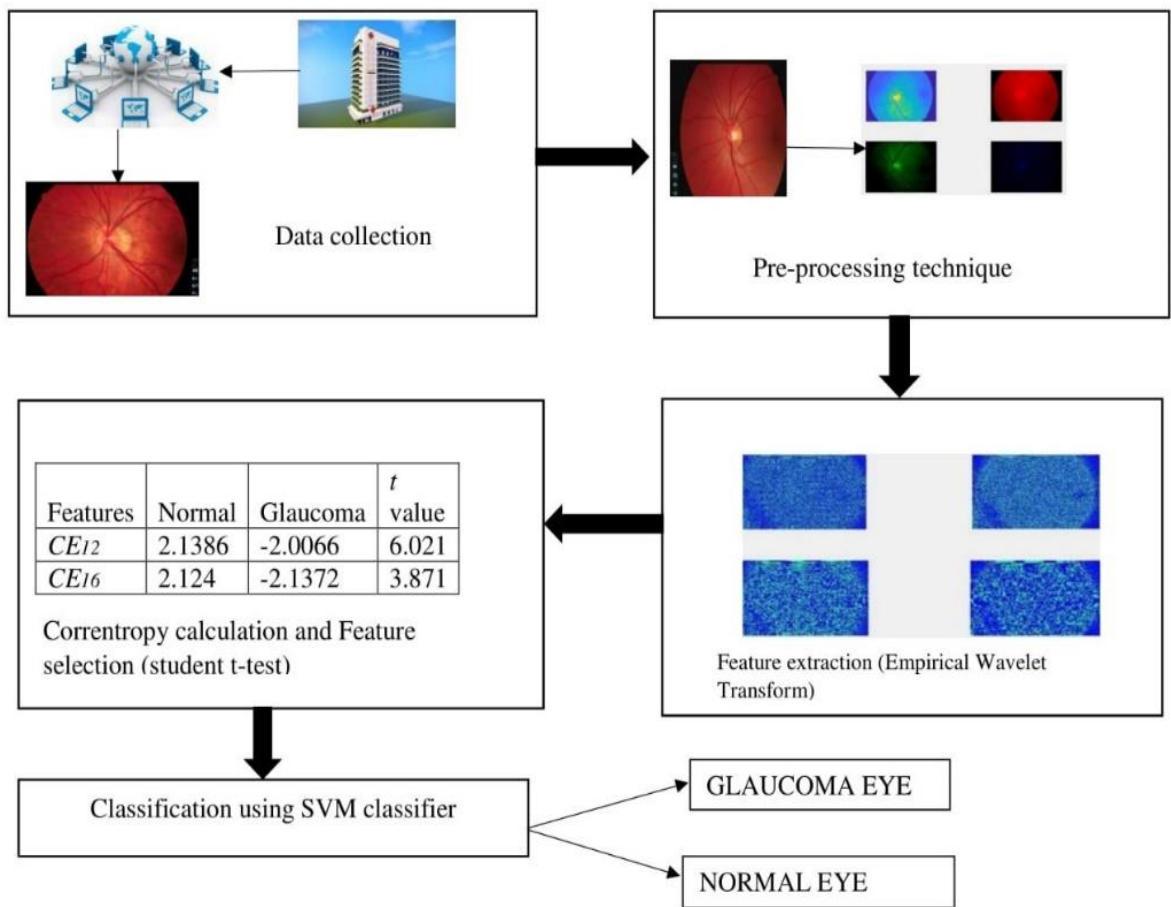
Figure 4.1: Implementation of Glaucoma detection using EWT and Correntropy features

(a)   **(b)**

Figure 4.2: (a) Glaucoma image (b) Normal image

Step 2: Pre-Processing:

It is the basic operation done on image in the detection process. Here, extraction of the 2D channels (Red, Green, Blue and Gray) from the 3D RGB fundus image is the pre-processing operation. Pseudo Color maps are applied on the channels for better visibility. These images are then pre-processed. Figure 4.3 and Figure 4.4 shows the extracted channels image from the fundus image.
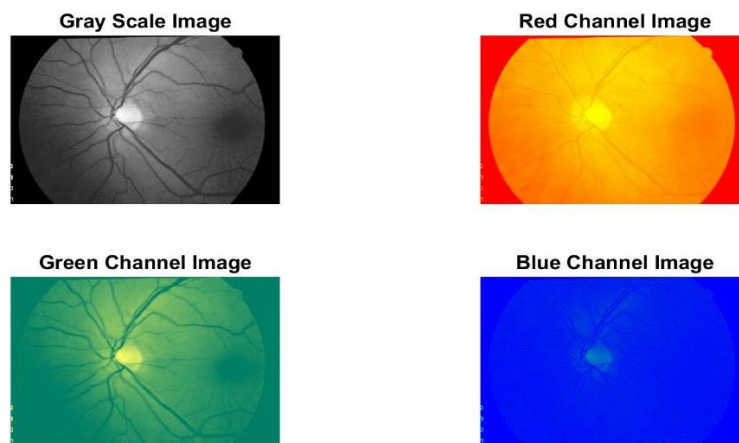
Figure 4.3: Extracted channels from the Glaucoma fundus image.
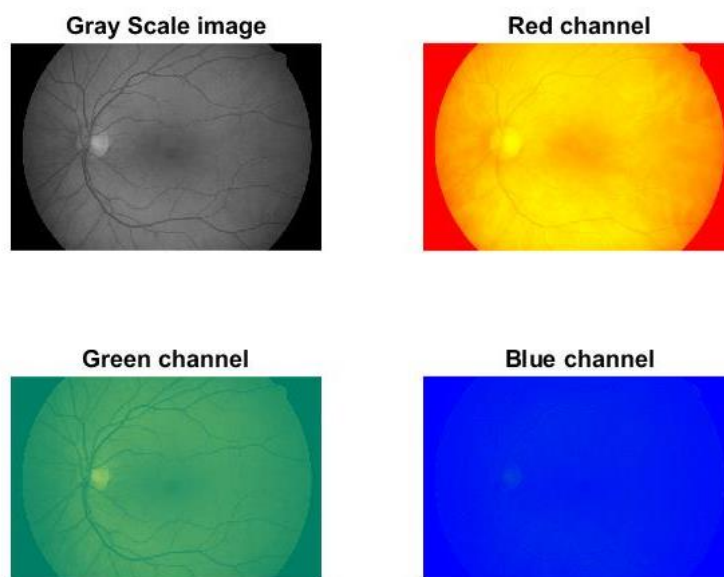
Figure 4.4: Extracted channels from the Normal fundus image.

Step 3: Feature Extraction:

Feature extraction is defined as method which is used to transform the recognizable detectable and non-detectable features into respective exact terminologies. EWT is used as the feature extraction technique as it has advantage over other methods discussed in chapter-3. Here, four types of 2D EWT are applied on the fundus image are:

a) 2D Littlewoods-Paley EWT
b) 2D Tensor EWT
c) 2D Curvelet EWT
d) 2D Ridgelet EWT

a) Algorithm for EWT 2D Little-wood Paley:

INPUT: Extracted channel images $h(x)$.

OUTPUT: Sub-band images W_g^{eLP} (n, x).

START

STEP 1: Compute the Pseudo-Polar FFT $F_P(h)(\theta_i, |\omega|)$ and take the average with respect to θ_i:

$$\widetilde{F_P(|\omega|)} = \frac{1}{N_\theta} \sum_{i=0}^{N_\theta - 1} |F_P(h)(\theta_i, |\omega|)| \qquad (14)$$

where θ_i is i_{th} Fourier boundary angle $\in [0, \pi]$ and N is the number of filter segments. $\widetilde{F_P(|\omega|)}$ is the average Pseudo-Polar FFT.

STEP 2: Filter bank B can be build by performing Fourier boundaries detection on $\widetilde{F_P(|\omega|)}$.

$$B = \{\phi_1(x), \{\psi_n(x)\}_{n=1}^{N-1}\} \qquad (15)$$

where $\phi_1(x)$ and $\psi_n(x)$ are filter bank parameters.

STEP 3: Pass extracted channel image $h(x)$ from the designed filter bank B to obtain the sub-band images W_g^{eLP} (n, x)

where W_g^{eLP} (n, x) is n^{th} EWT Littlewood Paley component.

END

Figure 4.5 and figure 4.6 shows the sub-band images obtained from the 2D littlewood-paley EWT.

Figure 4.5: EWT components of the Gray, Red, Blue and Green channel of the glaucoma affected fundus eye image

Figure 4.6: EWT components of the Gray, Red, Blue and Green channel of the normal fundus eye image.

b) Algorithm for EWT 2D Tensor:

INPUT : Extracted channel images $h(x)$.

OUTPUT: Sub-band images $W_g^{et}(n, x)$.

START
STEP 1: For each row i, compute its 1D FFT, then compute the average row spectrum magnitude

$$\tilde{F}_{row}(\omega_2) = \frac{1}{N_{row}} \sum_{i=0}^{N_{row}-1} |F_{1,x_1}(h)(i, \omega_2)| \qquad (16)$$

where $\tilde{F}_{row}(\omega_2)$ is the average 1D FFT of rows. $F_{1,x_1}(h)(i, \omega_2)$ is 1D FFT.

  STEP 2: For each column j, compute its 1D FFT \; then compute the average columns spectrum magnitude

$$\widetilde{F_{col}}(\omega_1) = \frac{1}{N_{col}} \sum_{i=0}^{N_{col}-1} |F_{1,x_2}(h)(\omega_1, j)| \qquad (17)$$

where $\widetilde{F_{col}}(\omega_1)$ is the average 1D FFT of columns. $F_{1,x_2}(h)(\omega_1, j)$ is 1D FFT.

STEP 3: Perform the Fourier boundaries detection on $\tilde{F}_{row}$ to get Ω row and build corresponding filter bank.

$$B_{row} = \{\phi_1^{row}, \{\psi_n^{row}\}_{n=1}^{N_R-1} \qquad (18)$$

where Ω row is the row Fourier boundaries, B_{row} is the row filter bank and ϕ_1^{row} and ψ_n^{row} are filter bank parameters.

STEP 4: Perform the Fourier boundaries on $\tilde{F}_{col}$ to get and Ω_{col} build corresponding filter bank

$$B_{col} = \{\phi_1^{col}, \{\psi_n^{col}\}_{n=1}^{N_C-1} \qquad (19)$$

where Ω_{col} is the column Fourier boundaries, B_{col} is the column filter bank and ϕ_1^{col} and ψ_n^{col} are filter bank parameters.

STEP 5: Filter $h(x)$ along the rows using filter bank obtain the N_R output images then Filter each previous output images along the columns to obtain N_c output images.

STEP 6: Obtain the sub-band images $W_g^{et}(n, x)$

where $W_g^{et}(n, x)$ is the nth Tensor component.

END

Figure 4.7 and Figure 4.8 shows the sub-band images obtained from the Tensor 2D EWT
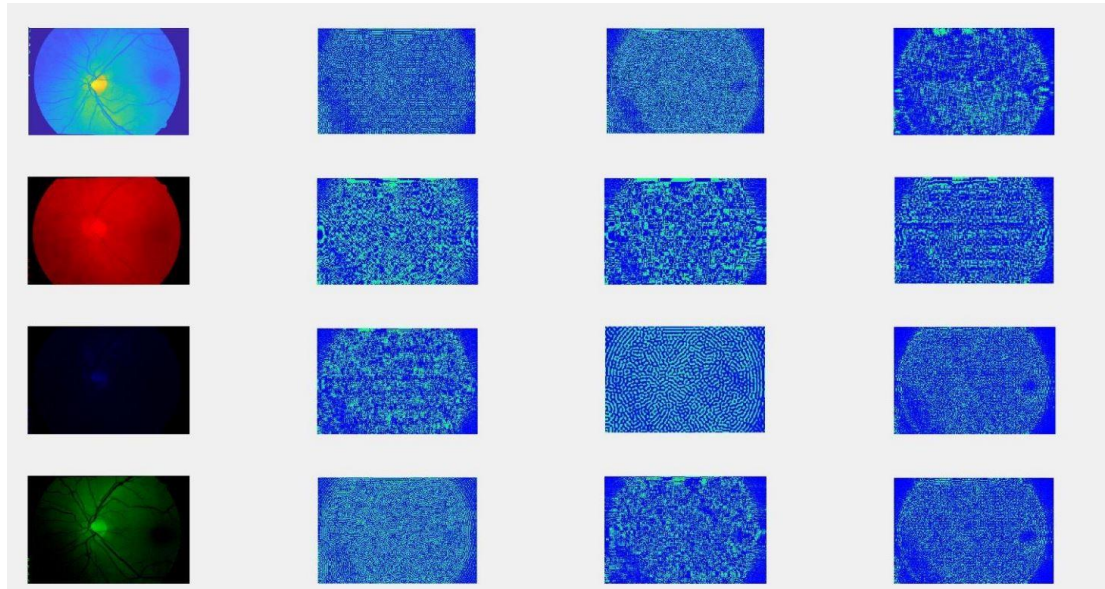

Figure 4.7: Tensor 2D EWT components of the Gray, Red, Blue and Green channel of the glaucoma affected fundus eye image.
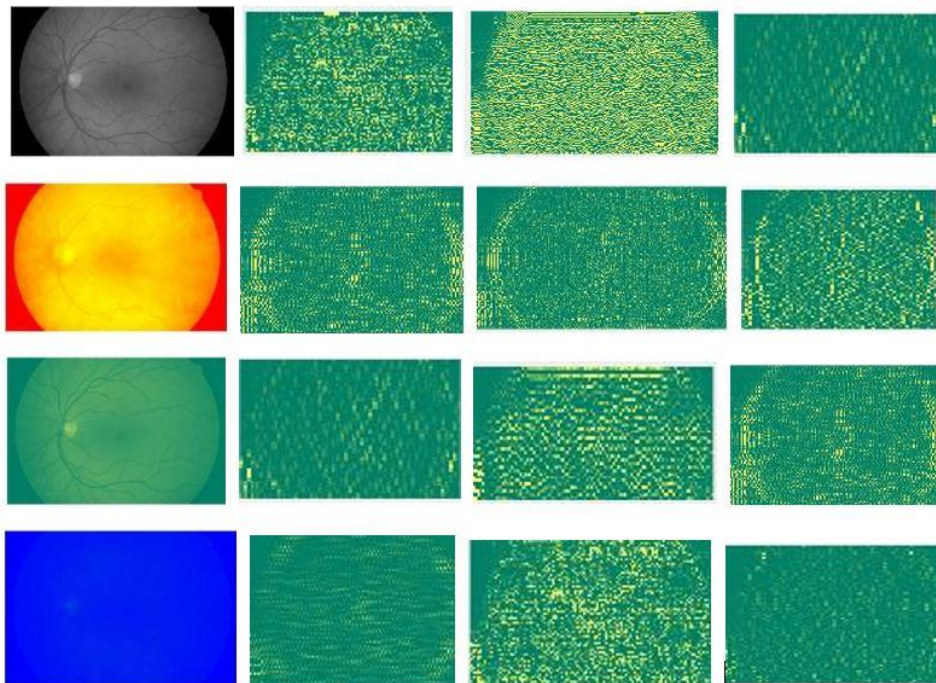
Figure 4.8: Tensor 2D EWT components of the Gray, Red, Blue and Green channel of the normal fundus eye image

c) Algorithm for EWT 2D Ridgelet:

INPUT : Extracted channel images $h(x)$.

OUTPUT: Sub-band images $W_g{}^{er}(n, \theta, x)$.

START

STEP 1: Compute the Pseudo-Polar FFT $F_P(h)(\theta_i, |\omega|)$ and take the average with respect to θ_i:

$$\widetilde{F_P(|\omega|)} = \frac{1}{N_\theta} \sum_{i=0}^{N_\theta - 1} |F_P(h)(\theta_i, |\omega|)| \tag{20}$$

where θ_i is i_{th} Fourier boundary angle ϵ $[0,\pi]$ and N is the number of filter segments. $\widetilde{F_P(|\omega|)}$ is the average Pseudo-Polar FFT.

STEP 2: Filter bank B can be build by performing Fourier boundaries detection on $\widetilde{F_P(|\omega|)}$

$$B = \{\phi_1(x), \{\psi_n(x)\}_{n=1}^{N-1}\} \tag{21}$$

where $\phi_1(x)$ and $\psi_n(x)$ are filter bank parameters.

STEP 3: Pass extracted channel image $h(x)$ from the designed filter bank B to obtain the sub-band images $W_g{}^{er}(n, \theta, x)$.

where $W_g{}^{er}(n, \theta, x)$ is n^{th} EWT Ridgelet component.

END

Figure 4.9 and Figure 4.10 shows the sub-band images obtained from the Ridgelet 2D EWT
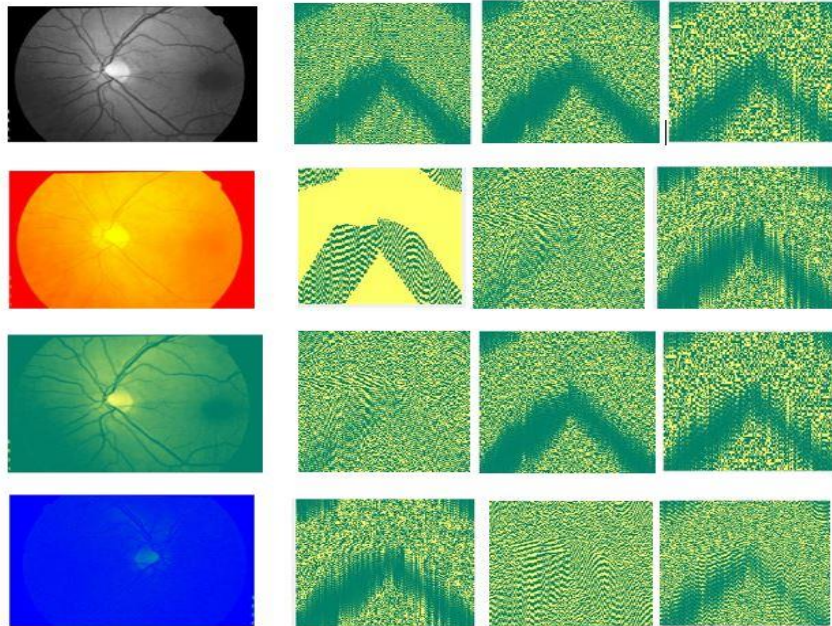
Figure 4.9: Ridgelet 2D EWT components of the Gray, Red, Blue and Green channel of the glaucoma affected fundus image eye
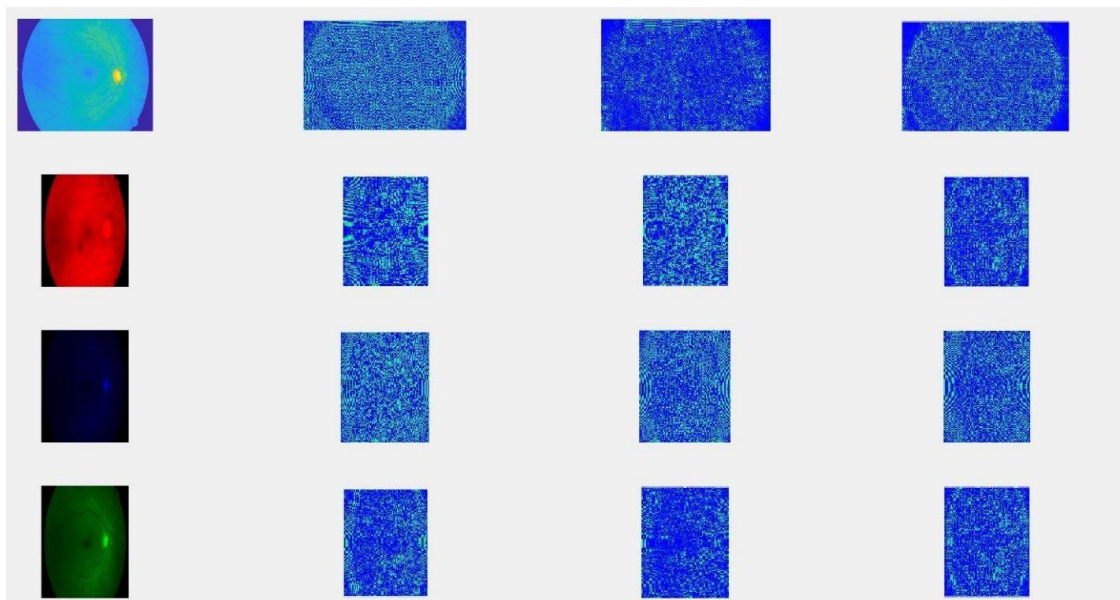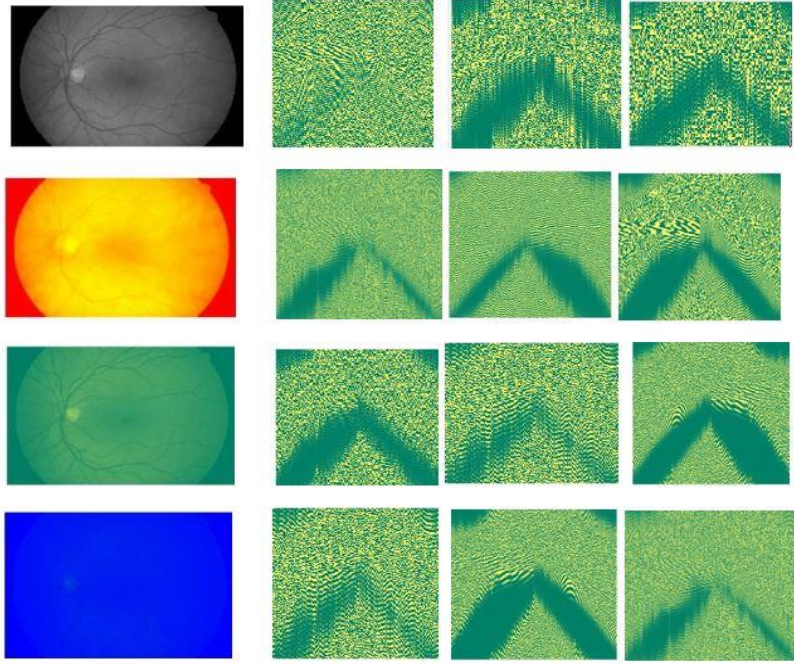
Figure 4.10: Ridgelet 2D EWT components of the Gray, Red, Blue and Green channel of the normal fundus image eye

d) **Algorithm for EWT 2D Curvelet:**

INPUT : Extracted channel images $h(x)$.

OUTPUT: Sub-band images W_g^{ec} (n, x).

START

STEP 1: Compute the Pseudo-Polar FFT $F_P(h)(\theta_i, |\omega|)$ and take the average with respect to θ_i:

$$\widetilde{F_P(|\omega|)} = \frac{1}{N_\theta} \sum_{i=0}^{N_\theta - 1} |F_P(h)(\theta_i, |\omega|)| \tag{22}$$

where θ_i is i_{th} Fourier boundary angle ϵ [0,π] and N is the number of filter segments. $\widetilde{F_P(|\omega|)}$ is the average Pseudo-Polar FFT.

STEP 2: Filter bank B can be build by performing Fourier boundaries detection on $\widetilde{F_P(|\omega|)}$

$$B = \{\phi_1(x), \{\psi_n(x)\}_{n=1}^{N-1}\} \tag{23}$$

where $\phi_1(x)$ and $\psi_n(x)$ are filter bank parameters.

STEP 3: Pass extracted channel image $h(x)$ from the designed filter bank B to obtain the sub-band images W_g^{ec} (n, x).

where W_g^{ec} (n, x) is n^{th} EWT Cuevelet component.

END

Figure 4.11 and Figure 4.12 shows the sub-band images obtained from the Curvelet 2D EWT
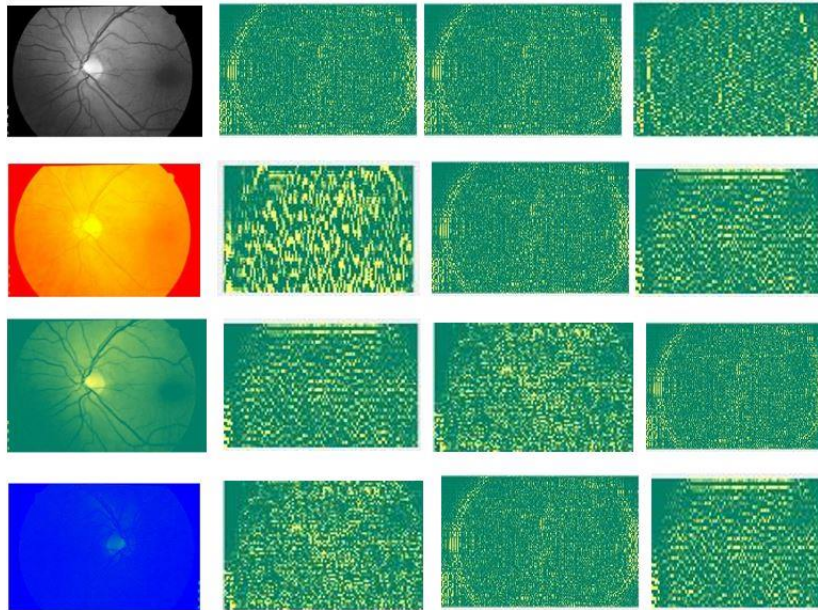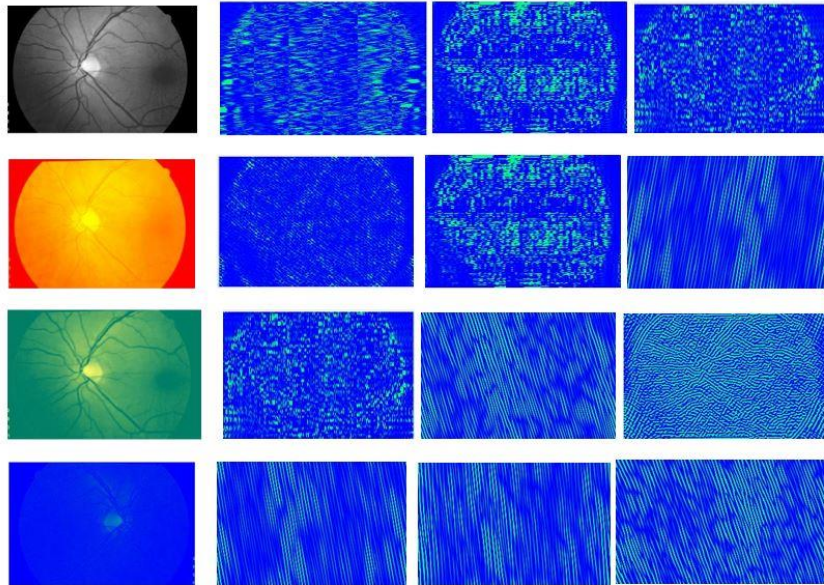

Figure 4.11: Curvelet 2D EWT components of the Gray, Red, Blue and Green channel of the glaucoma affected fundus eye image
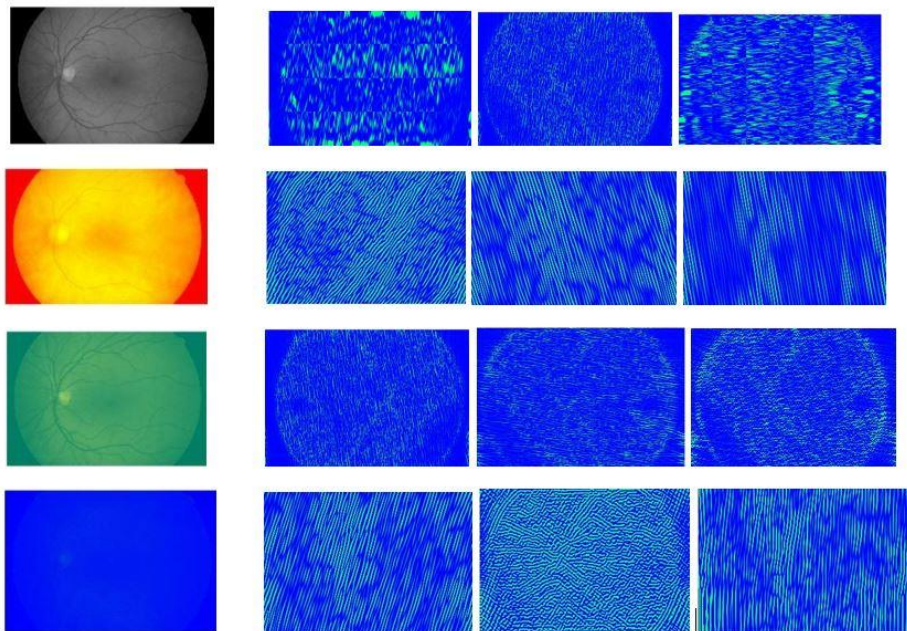
Figure 4.12: Curvelet 2D EWT components of the Gray, Red, Blue and Green channel of the normal fundus image eye

Figure 4.13 to Figure 4.16 shows the frequency spectrum of the image obtained from the Glaucoma and normal images obtained from the 2D Little-wood Paley, 2D Tensor EWT, 2D Ridgelet EWT and 2D Curvelet EWT respectively. For every different image these frequency spectrum is also different.

(a)   **(b)**
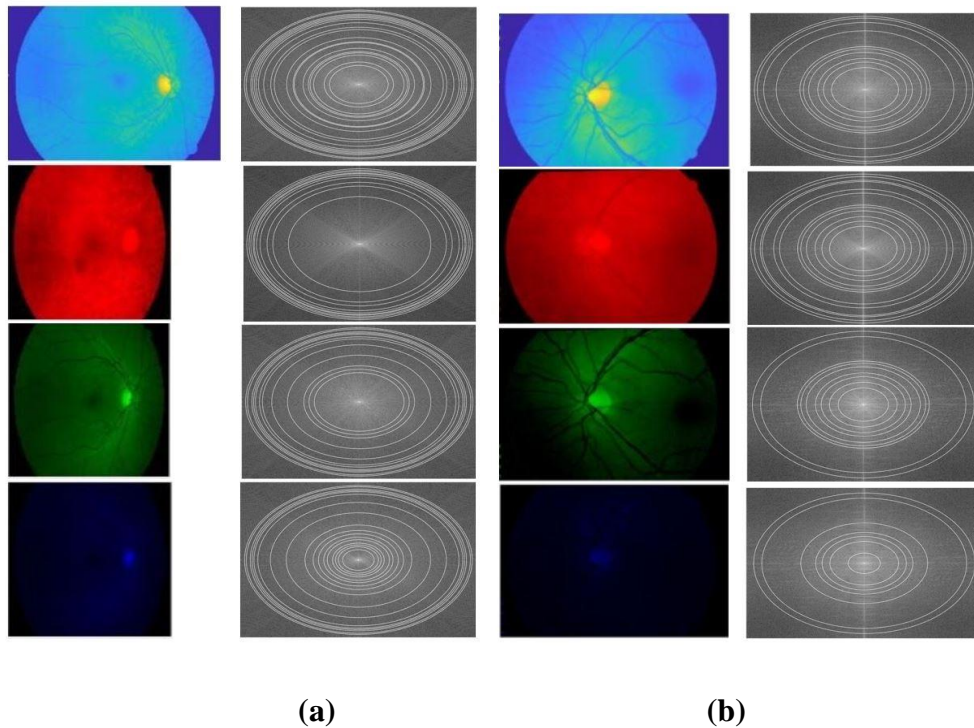
Figure 4. 13: Frequency spectrum of the (a) Glaucoma fundus image and (b) normal fundus image obtained by the 2D EWT Littlewood-paley.
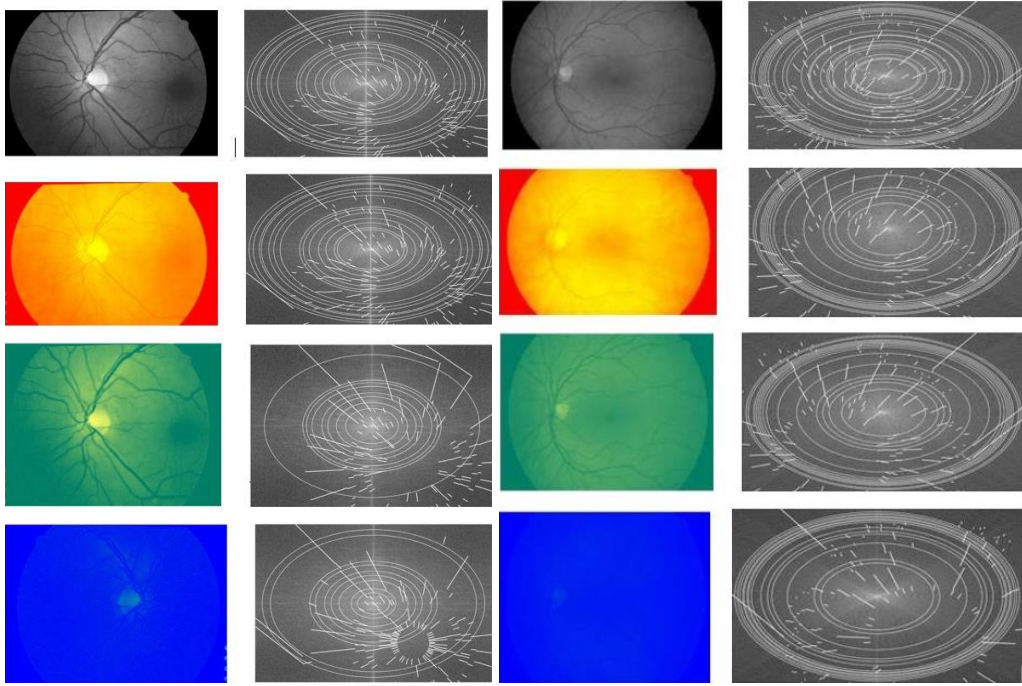
(a)   **(b)**

(b) Figure 4. 14: Frequency spectrum of the (a) Glaucoma fundus image and (b) normal fundus image obtained by the 2D EWT Curvelet.
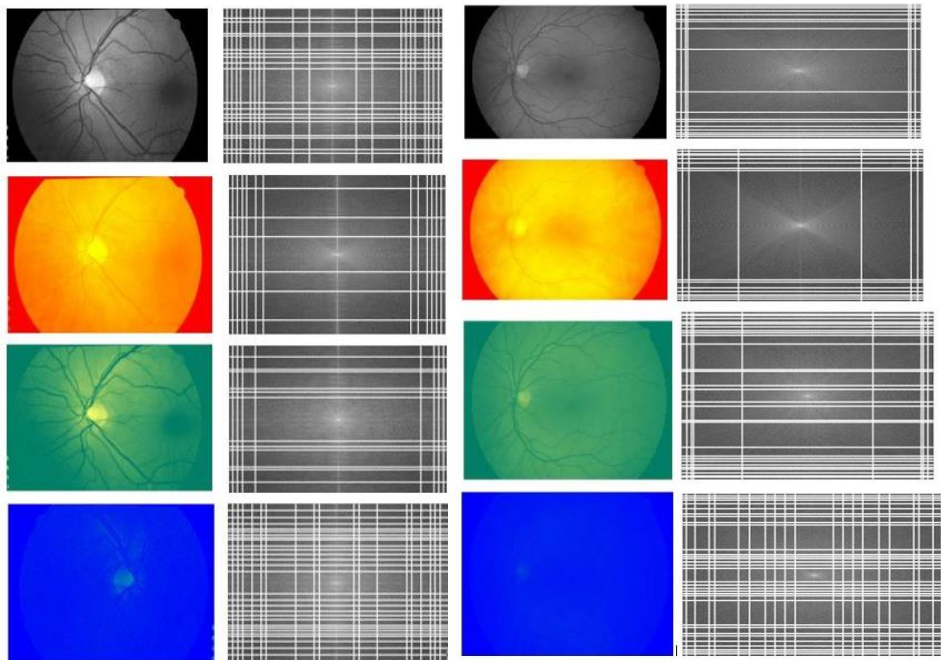
(a)   **(b)**

Figure 4. 15: Frequency spectrum of the (a) Glaucoma fundus image and (b) normal fundus image obtained by the 2D EWT Tensor.

(a)   **(b)**
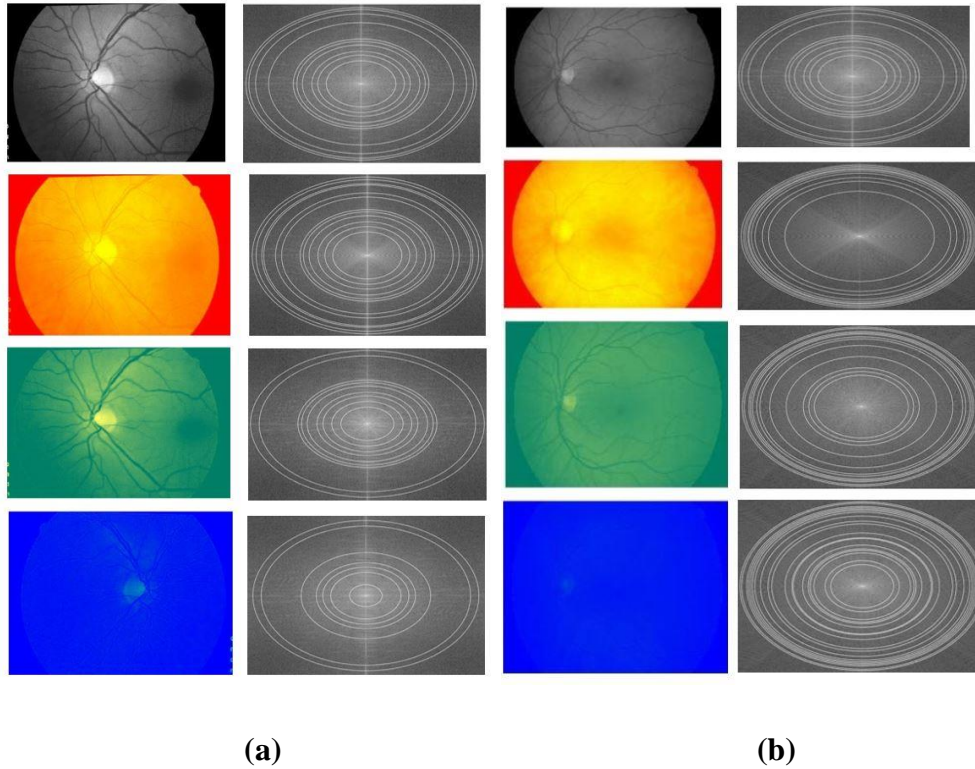
Figure 4. 16: Frequency spectrum of the (a) Glaucoma fundus image and (b) normal fundus image obtained by the 2D EWT Ridgelet.

The sub-band images are further processed for the calculation of correntropy feature.

Step 4: Feature Selection:

Student t-test algorithm is used as the feature selection technique in this method. In student t-test, normal distribution of values is done. The highest ranked values obtained from this method are used for the training the classifier which detects Glaucoma in the person. Correntropy feature values are calculated from the above obtained EWT components and then subjected to the student t-test algorithm for the feature selection. These values are given in the form of tabular form where the values are arranged in descending order of the t values calculated from the student t-test algorithm in which values are ranked accordingly. *CExy* is correntropy value of '*x*' EWT component of '*y*' image.

Table 4.1 to Table 4.4 shows the best 6 correntropy features for gray channel, green channel, red channel and blue channel respectively for Littlewood-paley 2D EWT.

48

Table 4.1: Feature Selection for Gray Channel

Features	Normal	Glaucoma	t value
CE_{32}	3.9549	-0.0487	5.731
CE_{56}	2.9486	-1.6788	3.463
CE_{15}	2.1386	-1.3295	2.139
CE_{34}	1.7233	-1.3744	1.746
CE_{45}	3.4563	-4.265	1.564
CE_{23}	2.3457	-2.365	0.989

Table 4.2: Feature Selection for Green Channel

Features	Normal	Glaucoma	t value
CE_{62}	2.0489	-2.0404	3.611
CE_{15}	1.0965	-1.0821	3.013
CE_{46}	0.4523	-0.4667	1.475
CE_{32}	1.7894	-1.6869	1.413
CE_{54}	2.3695	-1.2365	1.212
CE_{21}	3.2654	-0.2365	0.456

Table 4.3: Feature Selection for Red Channel

Features	Normal	Glaucoma	t value
CE_{31}	2.4587	-2.4371	4.856
CE_{33}	1.3273	-2.9073	4.318
CE_{25}	2.6547	-0.7853	3.176
CE_{13}	1.2321	-1.2716	2.156
CE_{22}	2.3651	-1.2637	2.026
CE_{51}	3.2635	-1.9586	1.562

Table 4.4 : Feature Selection for Blue Channel

Features	Normal	Glaucoma	t value
CE_{25}	2.1386	-2.0066	6.021
CE_{62}	2.124	-2.1372	3.871
CE_{12}	0.5319	-0.5498	2.059
CE_{36}	0.8765	0.8795	1.032
CE_{52}	2.321	-2.323	1.002
CE_{43}	1.2365	-1.2365	0.952

Table 4.5 to Table 4.8 shows the best 6 correntropy features for gray channel, green channel, red channel and blue channel respectively for Tensor 2D EWT.

Table 4.5: Feature Selection for Gray Channel

Features	Normal	Glaucoma	t value
CE_{61}	1.64867	-4.3381	v7.58758
CE_{26}	1.51341	-2.5189	7.25516
CE_{45}	0.25051	-4.1736	6.16615
CE_{12}	1.33649	-1.3447	5.16564
CE_{31}	0.09106	-0.9019	5.15116
CE_{33}	1.07879	-3.4004	4.02652

Table 4.6: Feature Selection for Green Channel

Features	Normal	Glaucoma	t value
CE_{11}	0.99108	-1.1143	4.44925
CE_{16}	0.81046	-1.5071	4.02616
CE_{25}	0.58251	-1.8442	3.91423
CE_{34}	1.15538	-1.3908	2.78025
CE_{64}	1.63895	-1.1091	1.93994
CE_{66}	1.43368	-0.9672	0.51061

Table 4.7: Feature Selection for Red Channel

Features	Normal	Glaucoma	t value
CE_{35}	0.44373	-1.4419	5.24792
CE_{23}	1.10135	-0.3939	5.11434
CE_{52}	0.78648	-0.371	4.08472
CE_{31}	0.39276	-1.0193	3.26543
CE_{22}	0.90779	-0.8645	2.94218
CE_{15}	1.51074	-0.1217	2.78977

Table 4.8 : Feature Selection for Blue Channel

Features	Normal	Glaucoma	t value
CE_{16}	1.46369	-0.6711	7.0816
CE_{26}	1.03138	-2.7105	6.56428
CE_{21}	1.20305	-3.0451	6.05194
CE_{63}	0.30425	-1.4422	3.91423
CE_{25}	0.46332	-3.5381	2.87557
CE_{34}	1.58594	-1.5448	1.80857

Table 4.9 to Table 4.12 shows the best 6 correntropy features for gray channel, green channel, red channel and blue channel respectively for Ridgelet 2D EWT.

Table 4.9: Feature Selection for Gray Channel

Features	Normal	Glaucoma	t value
CE_{15}	1.55017	-0.7867	2.53199
CE_{16}	1.52901	-1.3442	2.02503
CE_{64}	0.52616	-0.7265	1.92185
CE_{45}	0.54827	-0.885	1.48673
CE_{54}	0.02078	-1.1755	0.98607
CE_{13}	1.44413	-1.8118	0.38607

Table 4.10: Feature Selection for Green Channel

Features	Normal	Glaucoma	t value
CE_{46}	1.41202	-1.1123	7.25418
CE_{43}	1.40021	-0.6843	7.08111
CE_{51}	0.34245	-1.1371	6.07597
CE_{41}	1.48666	-1.5946	4.88588
CE_{62}	0.3926	-1.8092	3.88526
CE_{56}	0.56824	-0.7876	0.37709

Table 4.11: Feature Selection for Red Channel

Features	Normal	Glaucoma	t value
CE_{11}	0.79207	-0.2445	6.41052
CE_{66}	1.9614	-0.3439	6.36456
CE_{46}	1.46369	-1.4601	5.21581
CE_{33}	1.03138	-0.7522	4.02472
CE_{55}	1.20305	-1.2086	3.94062
CE_{56}	0.30425	-0.9749	3.62167

Table 4.12: Feature Selection for Blue Channel

Features	Normal	Glaucoma	t value
CE_{65}	0.96031	-4.1721	5.29667
CE_{26}	1.30999	-4.4065	3.12384
CE_{41}	1.1786	-0.5909	3.06149
CE_{36}	1.07453	-3.984	2.76713
CE_{42}	1.61179	-2.7047	2.25484
CE_{16}	0.99555	-1.2622	1.71351

Table 4.13 to Table 4.16 shows the best 6 correntropy features for gray channel, green channel, red channel and blue channel respectively for Curvelet 2D EWT.

Table 4.13: Feature Selection for Gray Channel

Features	Normal	Glaucoma	t value
CE_{23}	1.65115	-0.0487	5.731
CE_{65}	0.59253	-1.6788	3.463
CE_{51}	0.44647	-1.3295	2.139
CE_{43}	1.04677	-1.3744	1.746
CE_{54}	0.17963	-4.265	1.564
CE_{32}	0.31909	-2.365	0.989

Table 4.14: Feature Selection for Green Channel

Features	Normal	Glaucoma	t value
CE_{12}	0.40575	-2.0404	3.611
CE_{16}	-0.16246	-1.0821	3.013
CE_{64}	1.41202	-0.4667	1.475
CE_{53}	1.40021	-1.6869	1.413
CE_{35}	-0.34245	-1.2365	1.212
CE_{46}	1.48666	-0.2365	0.456

Table 4.15: Feature Selection for Red Channel

Features	Normal	Glaucoma	t value
CE_{13}	1.42858	-2.4371	4.856
CE_{43}	1.39559	-2.9073	4.318
CE_{56}	0.88827	-0.7853	3.176
CE_{63}	1.10305	-1.2716	2.156
CE_{64}	1.74681	-1.2637	2.026
CE_{22}	0.49159	-1.9586	1.562

Table 4.16: Feature Selection for Blue Channel

Features	Normal	Glaucoma	t value
CE_{44}	0.69999	-2.0066	6.021
CE_{35}	1.1314	-2.1372	3.871
CE_{55}	0.82474	-0.5498	2.059
CE_{61}	-0.90879	0.8795	1.032
CE_{13}	0.41058	-2.323	1.002
CE_{11}	-0.19379	-1.2365	0.952

Step 5: Classification

The way towards gathering the testing tests into the related classes is known as arrangement of dataset. Arrangement is sorted as regulated and unsupervised characterization. The SVM classifier goes under the class of regulated learning machine and chips away at the premise of number-crunching idea and factual hypothesis. SVM classifier can characterize both straight and non-direct order. After this step of feature selection, these values obtained from the all types of EWT were passed through the SVM classifier from where the cross validation accuracy and accuracy is calculated. The confusion matrix are obtained at k=5. Confusion matrix is a term given to a set of value written in the form of a matrix which is used to refer the performance of the classification model on a set of values (test data) for which the exact value are known. It gives us vision about the performance of an algorithm used. Table 4.17 to Table 4.20 shows the confusion matrix obtained from the SVM classifier.

Table 4.17: Confusion matrix for Tensor 2D EWT

		G	N
CM	G	142	18
	N	8	32

Table 4.18: Confusion matrix for Littlewood- Paley 2D EWT

CM		G	N
	G	129	20
	N	27	24

Table 4.19: Confusion matrix for Ridgelet 2D EWT

CM		G	N
	G	146	10
	N	15	29

Table 4.20: Confusion matrix for Curvelet 2D EWT

CM		G	N
	G	151	10
	N	11	29

In table 4.21, classification performance of the different types is done using the SVM classifier where different classification parameters like accuracy, cross-validation accuracy, sensitivity and specificity are calculated. Accuracy and sensitivity obtained from the Curvelet 2D EWT is highest i.e. 90% where the cross-validation accuracy obtained with fivefold of Littlewood 2D EWT is high i.e. 98.3% and specificity of Ridgelet 2D EWT is high i.e. 90.6% compared to other EWT transform methods.

Table 4.21:Comparison table of 4 Types of EWT

S.No.	EWT Types	Accuracy	Cross-validation accuracy	Specificity	Sensitivity
1.	Littlewood-Paley 2D EWT	76.5%	98.3%	0.8269	0.5454
2.	Tensor 2D EWT	87%	95.6%	0.8	0.8875
3.	Ridgelet 2D EWT	87.5%	97.8%	0.906	0.743
4.	Curvelet 2D EWT	90%	95.2%	0.8875	0.946667

Table 4.22 shows various techniques given for Glaucoma detection are compared with the results obtained from the implemented method where EWT 2D Little-wood Paley is used as feature extraction technique.

Table 4.22 : Comparison of different methods proposed for the detection of Glaucoma.

Authors	Methods given by authors	Images Number	Features extracted	Classifier	Accuracy (%)
Implemented work	Detection using texture features	250glaucoma/255 normals	Correntropy	SVM	98.3%
Krishnan *et al.* [24]	Detection using texture , DWT energy and HOS features	60 images	HOS and energy features	SVM	91.67%
Nyul *et al.* [25]	Glaucoma detection	NA	PCA	SVM	80%
Bock *et al.* [26]	Texture analysis for detection	NA	Pixel intensity values, FFT coefficients	SVM	86%

Mookiah *et al.* [27]	NA	NA	HOS and wavelet	SVM	95%
Dua *et al.*[28]	Detection using texture features	60 images	Energy signatures	SVM	93.33%
Beaula *et al.* [29]	Detection using texture features	NA	Correntropy	LS-SVM	96.6%
Patil *et al.* [30]	Using CDR	NA	CDR	SVM	NA
Dey *et al.* [31]	NA	NA	NA	SVM	96%
Singh *et al.* [32]	Detection of glaucoma	220 images	Red, Green and Blue values	SVM	97%

This work presents a method in which EWT is used as feature extraction technique. Correntropy features are extracted and features with the highest t values are used for the classification process. In this paper we have used SVM classifier. It can be concluded that EWT serves as an effective method for early stage detection of glaucoma. This paper compares different techniques given by different authors. The results obtained from the implemented method are compared with our technique where our method gives the highest accuracy of 98.3% using fivefold cross validation.

CHAPTER-5

CONCLUSION AND FUTURE SCOPE

Glaucoma is termed as neuro-degeneration of the optic nerve is one of the primary reason for vision impairment. Recovery of the degenerated nerve fibers of the optic nerve is difficult therefore, its early stage recognition and treatment is essential to prevent visual damage. In this work, we have compared the classification performance of the 2D Little-wood Paley EWT, Empirical Curvelet transform, Empirical Ridgelet Transform and Tensor 2D EWT for the Glaucoma detection in fundus images based on sensivity, specificity, accuracy and cross-validation accuracy. From the performance comparison, it has been found that the accuracy and sensitivity of the Empricial Curvelet Transform based method is higher whereas the fivefold cross-validation accuracy of the 2D Little-wood Paley EWT and specificity of Empirical Ridgelet transform is higher as compared to other EWT Transforms. The Empirical Curvelet Transform has the higher sensitivity so that its detection performance is also higher amongst the methods studied in this work. It can be also be concluded that EWT serves as an effective method for early stage detection of glaucoma. This work compares different techniques given by different authors.

The computational complexity is the main limitation of these techniques and in future, it can be enhanced. Also in future, this method can be extended for the analysis of OCT images and large database of fundus images for the detection of Glaucoma as well as for the detection of other diseases at early stage like Ovarian Cancer, Diabetics Retinopathy and Fatty Liver Detection.

REFRENCES

[1] https://byjus.com/biology/structure-of-eye/

[2]

http://www.medicinenet.com/imagecollection/eye_anatomy_detail_picture/picture.htm

[3] http://www.allaboutvision.com/conditions/

[4] https://www.glaucoma.org/glaucoma/normal-tension-glaucoma.php

[5] https://www.aao.org/eyenet/article/diagnosis-treatment-ofnormaltension-glaucoma

[6] https://www.emedicinehealth.com/normaltension_glaucoma/articem.html

[7] https://www.glaucoma.org/glaucoma/types-of-glaucoma.php

[8] https://wikivisually.com/wiki/Richard_Banister

[9] Hirschberg, J.-In Graefe-Saemisch, 2te. Aufl. Bd. 14, Abth. 1, S. 122, Leipzig, 1911.

[10] https://www.emedicinehealth.com/normal-tension_glaucoma/article_em.htm

[11] GBD 2015 Disease and Injury Incidence and Prevalence, Collaborators. (8 October 2016). "Global, regional, and national incidence, prevalence, and years lived with disability for 310 diseases and injuries, 1990–2015: a systematic analysis for the Global Burden of Disease Study 2015". Lancet. 388 (10053): 1545–1602

[12] Resnikoff, S., Pascolini, D., Etya'Ale, D., Kocur, I., Pararajasegaram, R., Pokharel, G.P. and Mariotti, S.P., 2004. Global data on visual impairment in the year 2002. *Bulletin of the world health organization*, *82*(11), pp.844-851.

[13] Quigley, H.A. and Broman, A.T., 2006. The number of people with glaucoma worldwide in 2010 and 2020. *British journal of ophthalmology*, *90*(3), pp.262-267.

[14] Agarwal, A., Gulia, S., Chaudhary, S., Dutta, M.K., Burget, R. and Riha, K., 2015, July. Automatic glaucoma detection using adaptive threshold based technique in fundus image. In *Telecommunications and Signal Processing (TSP), 2015 38th International Conference on* (pp. 416-420). IEEE.

[15] Pruthi, J. and Mukherjee, S., 2013. Computer based early diagnosis of glaucoma in biomedical data using image processing and automated early nerve fiber layer defects detection using feature extraction in retinal colored stereo fundus images. *International Journal of Scientific & Engineering Research*, *4*(4), pp.1822-28.

[16] Virk, J.K., Singh, M. and Singh, M., 2015, September. Cup-to-disk ratio (CDR) determination for glaucoma screening. In *Next Generation Computing Technologies (NGCT), 2015 1st International Conference on* (pp. 504-507). IEEE.

[17] Gopalakrishnan A., Almazroa A . , Raahemifar,K. Lakshminarayanan V. , "Optic Disc Segmentation using Circular Hough Transform and Curve Fitting " , 2nd International Conference on Opto-Electronics and Applied Optics (IEM OPTRONIX) , 2015

[18] Ayub J., Ahmad J., Muhammad J. , "Glaucoma Detection through Optic Disc and Cup Segmentation using K-mean Clustering" 2016 International Conference on Computing, Electronic and Electrical Engineering (ICE Cube)

[19] Sakthivel, Karthikeyan, and Rengarajan Narayanan. "An Automated Detection of Glaucoma Using Histogram Features." International Journal of Ophthalmology 8.1 (2015): 194–200. PMC. Web. 13 Nov. 2017.

[20] Kolar R., Jan J., Detection of glaucomatous eye via color fundus images using fractal dimensions, Radio Eng. 17 (3) (2008) 109–114.

[21]Acharya U.R., Dua S., Du X., Sree S.V., Chua C.K., Automated diagnosis of glaucoma using texture and higher order spectra features, IEEE Trans. Inf. Technology. Biomedical 15 (3) (2011) 449–455.

[22] Acharya U. R, Eugene Ng, E. Y. K. , Noronha L. W. J Min,, K. P., L. C. (2015). Decision support system for the glaucoma using Gabor transformation. Biomedical Signal Processing and Control, 15, 18-26.

[23] Shishir M., Ram Bilas P., Rajendra Acharya U, "Automated Diagnosis of Glaucoma Using Empirical Wavelet Transform and Correntropy Features Extracted From Fundus Images" , IEEE Journal Of Biomedical And Health Informatics, Vol. 21, No. 3, P.P. 803-813 , May 2017

[24] Krishnan M.,. M. R., & Faust, O. (2013). Automated glaucoma detection using hybrid feature extraction in retinal fundus images. Journal of Mechanics in Medicine and Biology, 13(01), 1350011.

[25] Nyúl L. G., (2009, October). Retinal image analysis for automated glaucoma risk evaluation. In Proc. of SPIE Vol (Vol. 7497, pp. 74971C-1).

[26] Bock R. Meier J., Nyl L. G., and Michelson G., "Glaucoma risk index: Automated glaucoma detection from color fundus images," Med. Image Anal., vol. 14, pp. 471–481, 2010

[27] Mookiah M. R. K., Acharya U. R., Lim C. M., Petznick A., and Suri J. S., "Data mining technique for automated diagnosis of glaucomausing higher order spectra and wavelet energy features," Knowl.-Based Syst., vol. 33, pp. 73–82, 2012.

[28] Dua S,., Acharya U. R,.,., Chowriappa P, & Sree, S. V. (2012). Wavelet-based energy features for glaucomatous image classification. Ieee transactions on information technology in biomedicine, 16(1), 80-87.

[29] Beaula L., Asirvatham M., Kalimuthu T. , "Earlier Detection of Glaucoma using Empirical Wavelet Transform" , International Journal for Research in Applied Science & EngineeringTechnology (IJRASET) , vol 5 , pp 1311-1316 , Apr 2017.

[30] . Patil H.P, Kamkhedhar V.S. , "Analysis of Human Retinal Images for Automated Glaucoma Screening" , International Journal for Research in Applied Science & EngineeringTechnology (IJRASET) , vol 2 , pp 371-377 , Dec 2014.

[31] Dey A and. Bandyopadhyay S K, "Automated Glaucoma Detection Using Support Vector Machine Classification Method," 2016, British Journal of Medicine & Medical Research (BJMMR), Kolkata

[32] Singh P and Marakarkandy B., (2017). Comparitive Study of Glucoma Detection using Different Classifiers.

[33] Tehmina Khalil, Samina Khalid and AdeelM.Syed "Review of Machine Learning Techniques for Glaucoma Detection and Prediction" Science and Information Conference 2014 August 27-29, 2014 | London, UK.8

[34] Trichonas G, Kaiser PK Optical coherence tomography imaging of macular oedema British Journal of Ophthalmology 2014;98:ii24-ii29.

[35] https://www.opsweb.org/?page=RetinalOCT

[36] Mary, M.C.V.S., Rajsingh, E.B. and Naik, G.R., 2016. Retinal fundus image analysis for diagnosis of glaucoma: a comprehensive survey. IEEE Access, 4, pp.4327-4354.

[37] https://www.ncbi.nlm.nih.gov/pmc/articles/PMC3131209/

[38] https://www5.cs.fau.de/research/data/fundus-images/

[39] Zhang, Z., Liu, J., Yin, F., Lee, B.H., Wong, D.W.K. and Sung, K.R., 2013, June. ACHIKO-K: Database of fundus images from glaucoma patients. In Industrial Electronics and Applications (ICIEA), 2013 8th IEEE Conference on (pp. 228-231). IEEE.

[40] http://www.ia.uned.es/~ejcarmona/DRIONS-DB.html

[41] Fumero, F., Alayón, S., Sanchez, J.L., Sigut, J. and Gonzalez-Hernandez, M., 2011, June. RIM-ONE: An open retinal image database for optic nerve evaluation. In Computer-Based Medical Systems (CBMS), 2011 24th International Symposium on (pp. 1-6). IEEE.

[42] http://medimrg.webs.ull.es/research/retinal-imaging/glaucoma/

[43] Dunham, M.H., 2006. Data mining: Introductory and advanced topics. Pearson Education India.

[44] Bhusri, S., Jain, S. and Virmani, J., 2016. Classification of breast lesions using the difference of statistical features. RESEARCH JOURNAL OF PHARMACEUTICAL BIOLOGICAL AND CHEMICAL SCIENCES, 7(4), pp.1365-1372.

[45] Rana S., Jain, S. and Virmani, J., 2016. Classification of Focal Kidney lesions using Wavelet-Based Texture Descriptors. International Journal of Pharma and Bio Sciences, 7(3), pp.646-652.

[46] Kumar, G. and Bhatia, P.K., 2014, February. A detailed review of feature extraction in image processing systems. In Advanced Computing & Communication Technologies (ACCT), 2014 Fourth International Conference on (pp. 5-12). IEEE.

[47] Aquino, A., Gegúndez-Arias, M.E. and Marín, D., 2010. Detecting the optic disc boundary in digital fundus images using morphological, edge detection, and feature extraction techniques. IEEE transactions on medical imaging, 29(11), pp.1860-1869.

[48] Li, H. and Chutatape, O., 2004. Automated feature extraction in color retinal images by a model based approach. IEEE Transactions on biomedical engineering, 51(2), pp.246-254.

[49] Jambholkar, T., Gurve, D. and Sharma, P.B., 2015, September. Application of Empirical Wavelet Transform (EWT) on images to explore Brain Tumor. In Signal Processing, Computing and Control (ISPCC), 2015 International Conference on (pp. 200-204). IEEE.

[50] Gilles, J., 2013. Empirical wavelet transform. IEEE transactions on signal processing, 61(16), pp.3999-4010.

[51] Thirumala, K., Umarikar, A.C. and Jain, T., 2015. Estimation of single-phase and three-phase power-quality indices using empirical wavelet transform. IEEE Transactions on power delivery, 30(1), pp.445-454.

[52] Liu, W., Cao, S. and Chen, Y., 2016. Seismic time–frequency analysis via empirical wavelet transform. IEEE Geoscience and Remote Sensing Letters, 13(1), pp.28-32.

[53] Maheshwari, S., Pachori, R.B. and Acharya, U.R., 2017. Automated diagnosis of glaucoma using empirical wavelet transform and correntropy features extracted from fundus images. IEEE journal of biomedical and health informatics, 21(3), pp.803-813.

[54] Gilles, J., Tran, G. and Osher, S., 2014. 2D empirical transforms. Wavelets, ridgelets, and curvelets revisited. SIAM Journal on Imaging Sciences, 7(1), pp.157-186.

[55] Huang, N.E., Shen, Z., Long, S.R., Wu, M.C., Shih, H.H., Zheng, Q., Yen, N.C., Tung, C.C. and Liu, H.H., 1998, March. The empirical mode decomposition and the Hilbert spectrum for nonlinear and non-stationary time series analysis. In Proceedings of the Royal Society of London A: mathematical, physical and engineering sciences (Vol. 454, No. 1971, pp. 903-995). The Royal Society.

[56] Gunduz, A. and Principe, J.C., 2009. Correntropy as a novel measure for nonlinearity tests. Signal Processing, 89(1), pp.14-23.

[57] Santamaría, I., Pokharel, P.P. and Principe, J.C., 2006. Generalized correlation function: definition, properties, and application to blind equalization. IEEE Transactions on Signal Processing, 54(6), pp.2187-2197.

[58] Liu, W., Pokharel, P.P. and Príncipe, J.C., 2007. Correntropy: Properties and applications in non-Gaussian signal processing. IEEE Transactions on Signal Processing, 55(11), pp.5286-5298.

[59] He, R., Zheng, W.S. and Hu, B.G., 2011. Maximum correntropy criterion for robust face recognition. IEEE Transactions on Pattern Analysis and Machine Intelligence, 33(8), pp.1561-1576.

[60] Jain S., 2016. Regression analysis on different mitogenic pathways. Network Biology, 6(2), p.40.

[61] Jain S., 2016. Mathematical Analysis using Frequency and Cumulative Distribution functions for Mitogenic Pathway. RESEARCH JOURNAL OF PHARMACEUTICAL BIOLOGICAL AND CHEMICAL SCIENCES, 7(3), pp.262-272.

[62] Virmani J., Kumar, V., Kalra, N. and Khandelwal, N., 2013. SVM-based characterisation of liver cirrhosis by singular value decomposition of GLCM matrix. International Journal of Artificial Intelligence and Soft Computing, 3(3), pp.276-296.

[63] Jain S., Naik, P.K. and Bhooshan, S.V., 2011, October. Non Linear Modeling of Cell Survival/Death Using Artificial Neural Network. In Computational Intelligence and Communication Networks (CICN), 2011 International Conference on (pp. 565-568). IEEE.

[64] Jain S. and Chauhan, D.S., 2015. Mathematical analysis of receptors for survival proteins. International Journal of Pharma and Bio Sciences, 6(3), pp.164-176.

[65] Jain, S. and Chauhan, D.S., 2016. Linear and Nonlinear Modeling of Protein Kinase B/AkT. In Proceedings of International Conference on ICT for Sustainable Development(pp. 81-88). Springer, Singapore.

[66] Jain, S., 2012. Communication of Signals and Responses Leading to Cell Survival Cell Death Using Engineered Regulatory Networks.

[67] Ning C.P., Ji, Q.L., Fang, S.B., Wang, H.Q., Zhong, Y.M. and Niu, H.T., 2018. Distribution patterns of microcalcifications in suspected thyroid carcinoma: a classification method helpful for diagnosis. European radiology, pp.1-8.

[68] Westner B.U., Dalal, S.S., Hanslmayr, S. and Staudigl, T., 2018. Across-subjects classification of stimulus modality from human MEG high frequency activity. PLoS computational biology, 14(3), p.e1005938.

[69] Jain, S., 2018. Classification of Protein Kinase B using discrete wavelet transform. International Journal of Information Technology, 10(2), pp.211-216.

PUBLICATIONS FROM THIS RESEARCH